The regulation of the homeostasis and regeneration of peripheral nerve is distinct from the CNS and independent of a stem cell population

Salome Stierli[1], Ilaria Napoli[1], Ian J White[1], Anne-Laure Cattin[1], Anthony Monteza Cabrejos[1], Noelia Garcia Calavia[1], Liza Malong[1], Sara Ribeiro[1], Julie Nihouarn[1], Richard Williams[1], Kaylene M Young[3], William D Richardson[4] and Alison C Lloyd[1,2]*

[1]MRC Laboratory for Molecular Cell Biology, University College London, Gower Street, London, WC1E 6BT

[2]UCL Cancer Institute, University College London, Gower Street, London, WC1E 6BT

[3]Menzies Institute for Medical Research, University of Tasmania, Hobart TAS 7000 Australia

[4]Wolfson Institute for Biomedical Research, UCL, Gower Street, London, WC1E 6BT

* corresponding author: alison.lloyd@ucl.ac.uk

Key words: tissue homeostasis, tissue regeneration, stem cells, PNS, CNS, Schwann cells.

Summary statement

Lineage analysis and long-term labelling studies show that peripheral nerve regeneration is underpinned by the proliferative plasticity of mature cells rather than the activation of a stem cell population.

Abstract

Peripheral nerves are highly regenerative in contrast to the poor regenerative capabilities of the CNS. Here we show that adult peripheral nerve is a more quiescent tissue than the CNS, yet all cell-types within a peripheral nerve proliferate efficiently following injury. Moreover, whereas oligodendrocytes are produced throughout life from a precursor pool, we find that the corresponding cell of the PNS, the myelinating Schwann cell (mSC) does not turnover in the adult. However, following injury, all mSCs can dedifferentiate to the proliferating progenitor-like SCs that orchestrate the regenerative response. Lineage analysis shows these newly-migratory, progenitor-like cells redifferentiate to form new tissue at the injury site, maintain their lineage but can switch to become a non-myelinating SC. In contrast, increased plasticity is observed during tumourigenesis. These findings show that peripheral nerves have a distinct mechanism for maintaining homeostasis and can regenerate without the need for an additional stem cell population.

Introduction

Once formed in the adult, peripheral nerves are relatively stable structures befitting of their role in transmitting signals back and forth between tissues and organs and the central nervous system (CNS). However, in contrast to the CNS, peripheral nerves are able to regenerate following an injury (Mahar and Cavalli, 2018). This requires not only the regrowth of the neurons but the creation of new tissue to repair the wound site, together with the remodelling of the remaining nerve tissue to provide an environment conducive for axonal regrowth (Cattin and Lloyd, 2016; Zochodne, 2012). Critical to this regenerative process is the main glial cell of the peripheral nervous system (PNS), the Schwann cell (SC). In the adult, SCs exist in one of two states: myelinating Schwann cells (mSCs), which myelinate larger axons in a 1:1 ratio and non-myelinating Schwann cells (nmSCs), which bundle together groups of smaller axons in structures known as Remak bundles (Harty and Monk, 2017; Monk et al., 2015). Following injury, these highly specialised cells have the capacity to dedifferentiate to a proliferating, progenitor-like SC, which orchestrates the regenerative response (Jessen and Mirsky, 2016; Napoli et al., 2012). The roles of SCs in this process include guiding regrowing axons across the injury site (Cattin et al., 2015; Parrinello et al., 2010), opening of the Blood Nerve Barrier (BNB) and the control of the inflammatory response (Napoli et al., 2012), remodelling the nerve environment (Brosius Lutz et al., 2017) and promoting the growth and survival of the regrowing axons (Arthur-Farraj et al., 2012; Fontana et al., 2012). Once the axons have regrown, the dedifferentiated SCs are thought to redifferentiate in response to axonal signals and the regenerative state resolves to return to the homeostatic state (Cattin and Lloyd, 2016; Zochodne, 2008).

The behaviour of mSCs is in stark contrast to the comparable cell of the CNS, the oligodendrocyte (OL). Once an oligodendrocyte has myelinated a neuron, it is post-mitotic in that it cannot return to a proliferative state. Moreover, new OLs are produced throughout life, either to replace OLs or to myelinate previously unmyelinated axon segments (Birey et al., 2017; Young et al., 2013). This de-novo myelination in adulthood is thought to contribute to the plasticity of the brain in processes such as learning and memory (Kaller et al., 2017; McKenzie et al., 2014). New OLs are produced from a continuously slowly- proliferating pool of progenitor cells that exist throughout the CNS, known as oligodendrocyte progenitor cells (OPCs) (Dimou and Simons, 2017; Kang et al., 2010). These cells continuously produce new OLs in the adult (Young et al., 2013) and following demyelination events in pathologies such as multiple sclerosis (Domingues et al., 2016).

It is not clear why the CNS and PNS have evolved distinct mechanisms to produce new cells and have such different regenerative capabilities. Moreover, the apparent lack of a stem cell/progenitor population in the PNS to produce new cells, either during homeostasis or following injury is unusual for a mammalian tissue. This has led to speculation that an

additional stem cell population contributes to the production of new SCs during the regenerative process (Amoh et al., 2005; Chen et al., 2012; McKenzie et al., 2006) and that SCs retain some of the multipotency that SC precursors exhibit during development in order to regenerate new nerve tissue (Petersen and Adameyko, 2017). In this study, we have characterised the behaviour of all cell types within peripheral nerve during homeostasis and during the regenerative process. Moreover, we have used lineage analysis to track the behaviour and fate of mSCs. We find that peripheral nerve is a highly quiescent tissue and that in contrast to OLs, mSCs do not turnover in adulthood. Following injury however, all cell types within the nerve proliferate with close to 100% of mSCs entering the cell-cycle to become migratory, progenitor-like SCs, which orchestrate the multicellular nerve regeneration process without the requirement for a distinct SC stem cell population. Lineage analysis shows that these "repair" SCs retain the SC lineage but can switch from a mSC to a nmSC. In contrast, we find this restriction breaks down during SC tumourigenesis when these cells show increased plasticity. This work shows that peripheral nerve is a tissue with a distinct mechanism for both maintaining homeostasis and regenerating following injury- in that cells rarely turnover in the homeostatic state, whereas all cells in the tissue proliferate and contribute to the repair of the damaged nerve. This study also demonstrates the remarkable stability of glia in the PNS despite retaining the ability to efficiently convert to a progenitor-like SC following injury, providing a further illustration of the diversity of stem/progenitor cell phenotypes that exist in mammalian tissues.

Results

Identification of the cell composition of peripheral nerve

In order to determine the composition and turnover of cells found in a peripheral nerve, we initially systematically determined the cell composition within the endoneurium of mouse sciatic nerve. To do this, we used a number of transgenic mice with lineage-specific expression of fluorescent labels, along with immunostaining of endogenous markers to quantify the prevalence of each cell type using immunofluorescence (IF) and electron microscopy (EM) analysis. Consistent with previous findings (Salonen et al., 1988), we found that the vast majority of cells within the sciatic nerve are SCs (~ 70%), as determined by both staining with the cytoplasmic SC marker S100 and by EM analysis (Figure 1A-B). Moreover, these results were confirmed by imaging nerve sections from a transgenic mouse in which all SCs express eGFP (PLP-eGFP mice) (Figure 1A), (Mallon et al., 2002) and by immunostaining for myelin protein zero (P0) (Figure S1A) and p75 (Figure S1B). This analysis also confirmed that the majority of cells were mSCs (51%) with the ratio of mSCS to nmSCs (21%) roughly 2:1 (Figures 1B-C and S1C).

P75 has been used extensively as a marker to label both nmSCs and the dedifferentiated SCs that form following an injury (Jessen et al., 2015). However, we also found a significant proportion of p75+ cells that did not appear to be associated with axons and had a distinct elongated morphology (Figure 1D). Moreover, these p75+ cells did not express eGFP in nerves isolated from PLP-eGFP mice (Figure 1D) or tdTomato in nerves from P0-Cre:TdTomato mice that express tdTomato in all SCs (Figure S1D). Instead, we found that these cells (p75+/eGFP-), expressed the commonly used markers for pericytes, NG2 and PDGFRβ (Figure 1D) (Armulik et al., 2011). Moreover, we confirmed NG2 expression in these cells by analysing nerves from mice that express dsRed by virtue of an NG2-driven expression construct (NG2-dsRed mice) (Zhu et al., 2008) and found a complete overlap between NG2/ PDGFRβ immunostaining and dsRed expression (Figures 1D andS1E).

We could distinguish three populations of NG2+/ PDGFRβ+ cells within the nerve endoneurium. The first population (1.5% of total cells within the endoneurium) had all the characteristics of classical pericytes. They co-expressed NG2 and PDGFRβ (not shown), were negative for p75 and expressed α-smooth muscle actin (αSMA) (Figure 1D). Moreover, they were found tightly associated around blood vessels (CD31+ cells) (Figure 1D) consistent with a pericyte population that could be observed within the basal lamina around the blood vessels by EM (Figure S1F). A much larger population of NG2+/ PDGFRβ+cells (12.5%), were p75+ (Figure 1C). They were also S100- (Figure S1G) and were not labelled in either PLP-eGFP mice or in P0-Cre:tdTomato mice (Figures 1D and S1D) and so appeared not to be SCs or derived from SCs. We also noticed that a proportion of these cells were found loosely associated with blood vessels (4.5%) (Figure 1D), whereas others appeared to be within the endoneurium away from blood vessels (Figures 1D and S1E), and so while unable to distinguish these two populations by markers, we classified them as blood vessel associated (4.5%) or blood vessels non-associated (8%) (Figures 1C and S1C). It is important to note that EM analysis showed that while some of these cells were associated with blood vessels, they were not found within the basal lamina of the vessels (Figure S1H). EM analysis also showed high amounts of endoplasmic reticulum within these cells indicating that they are cells that have provisionally been identified as neural crest-derived fibroblasts by others (Joseph et al., 2004) (Figure S1H).

The remaining cells of peripheral nerve were shown to be endothelial cells (6%, CD31+) and macrophages (8%, F480+/Iba1+) (Figures 1C and S1C). We did not detect other inflammatory cells such as mast cells, neutrophils or dendritic cells within the uninjured nerves (not shown). In conclusion, we have been able to identify all cell types within the endoneurium of the nerve and have characterised the tools to enable us to trace their behaviour in normal nerve and following injury.

Myelinating Schwann cells do not proliferate in the adult

The CNS is relatively quiescent compared to many tissues of the body, however, cumulative long-term EdU labelling studies have shown that essentially all OPCs proliferate, albeit slowly, with turnover times ranging from ~1 week to >1 month in different regions of the brain, spinal cord and optic nerve (Young et al., 2013). To determine the overall proliferation rate of cells within the endoneurium of peripheral sciatic nerve, we used the same protocol of cumulative EdU labelling to mark proliferating cells in adult mice. For each time point (8, 30 and 70 days), we calculated the percentage of cells that had accumulated EdU and this increased in a linear manner over time showing that the proliferation rate remained constant during early adulthood (Figure 2A). However, the overall proliferation rate was very low (~0.8% per week), with fewer than 10% of the cells labelled within the 70 day time period. This implies that if all cells within the nerve were proliferating at the same rate, the tissue turnover time would be ~2.4 years. These findings highlight the quiescent nature of peripheral nerve.

To determine the identity of the proliferating cells within the nerve, we used the cell type specific markers defined above (Figures 2B and S2A). Analysis of the long-term labelling studies showed that mSCs appeared to be completely quiescent, as we failed to detect a single EdU+ mSC over the 70 day-labelling period. This implies that mSCs, once formed, do not turnover. In contrast, we detected a very low level of EdU+ nmSCs in Remak bundles (Figure 2B). We confirmed the identity of these cells by the detection of EdU+/ eGFP+ cells in EdU-dosed PLP-eGFP mice (Figures 2C and S2B) and the association of EdU+ nuclei within eGFP+ Remak structures in 3D reconstructions (Movie S1). However, we found that the nmSC turnover rate was extremely slow (~72 months) (Figure 2D). Thus the glial cells of the PNS show very different proliferative dynamics to the corresponding cells of the CNS. No new mSCS and very few new nmSCs are produced in the adult, whereas new oligodendrocytes are produced throughout life (Young et al., 2013).

The most highly proliferative cell-type in peripheral nerve was the resident macrophages, with a turnover time of approximately 4 months (Figures 2D and S2A). This is somewhat similar to the turnover rate of the resident macrophage population (microglia) in the brain (Askew et al., 2017; Tay et al., 2017). All other cell types also showed low but detectable levels of turnover, with endothelial cells, NG2+/PDGFRβ+/p75+/αSMA- cells and pericytes showing approximate turnover rates of 15, 7.5 and 6 months respectively (Figure 2D and S2A).

All myelinating Schwann cells proliferate following injury

The analysis of homeostatic peripheral nerve demonstrated a mostly quiescent tissue consistent with its stable architecture. However, peripheral nerves are highly regenerative requiring that the tissue retains plasticity. Following an injury, the distal stump of the nerve undergoes extensive breakdown, followed by clearance of debris, regrowth and remodelling to reform a functional nerve (Cattin and Lloyd, 2016; Zochodne, 2008). SCs have a key role in orchestrating the regenerative process and have been reported to dedifferentiate following injury to pursue this role (Cattin and Lloyd, 2016; Jessen and Mirsky, 2016). However, it remains unclear whether all SCs have this capacity, whether a smaller "stem-like" compartment is involved or whether new SCs derive from other stem cell compartments to regenerate the nerve**.** To distinguish between these possibilities, we performed lineage analysis using a transgenic mouse, which allows Cre expression to be specifically induced in mSCs in the adult (P0-CreER^{T2}:YFP) following tamoxifen administration (Leone et al., 2003; Ribeiro et al., 2013).

To analyse the initial stages of the regenerative process and to investigate the proliferative potential of mSCs, we performed cumulative EdU labelling following sciatic nerve transection in P0-CreER^{T2}:YFP adult mice, 14 days following tamoxifen treatment (Figure 3A). Analysis of the distal stump (downstream of the cut and the newly-formed bridge region) showed a dramatic switch in the proliferative status of the nerve with > 80% of cells within the nerve accumulating EdU by Day 8 following injury (Figure 3A). Remarkably, despite being completely quiescent in the adult nerve, >80% of the YFP+ (mSC-derived) cells in the nerve proliferated within 6 days of the injury with close to 100% proliferating by Day 10. This result showed that, despite being completely quiescent in the adult, all mSCs have the capacity to proliferate following an injury (Figures 3A and S3A).

In order to determine the kinetics of mSC proliferation following an injury, we performed EdU pulse labelling after nerve transection and found that the peak of mSC proliferation was at Day 4 following injury with the rates returning to lower but still detectable levels at Day 8-10 following injury (Figures 3B and S3B). Total cell proliferation followed a similar trend demonstrating a robust proliferative burst of all the identified cell types within the nerve, as the myelin structures break down within the injured nerve (Figures 3B and S3C). Notably, the endothelial cells in the distal stump did not enter the cell-cycle until after Day 4, indicating that at this time point, new blood vessels have not formed within the distal stump. This is in contrast to what was reported previously for the bridge region of a transected nerve, where newly-formed blood vessels have an important role in the regenerative process (Cattin et al., 2015). This analysis also showed there was an increase in the proportion of two cell types within the nerve: macrophages that increased from 8% to 22%, following the recruitment of

monocytes from the blood stream and NG2+, PDGFRβ+, αSMA- cells that increased from 12% to 22%, reflecting the higher proliferative rate of this cell type (Figures 3C and S3D). Furthermore, neutrophils and other inflammatory cells are recruited into regenerating nerve, most likely accounting for the minor unknown cell population at this time point (Napoli et al., 2012).

A critical aspect of SC behaviour during the regeneration of a transected nerve is that they become migratory, forming cellular cords that transport regrowing axons across the injury site (Parrinello et al., 2010). However, it is not clear whether both nmSCs and mSCs are able to undergo this marked change in migratory behaviour. To track the migration of individual SCs, we administered tamoxifen to P0-CreER^{T2}:Confetti mice (Snippert et al., 2010) so that individual mSCs stochastically expressed a combination of four fluorophores (nuclear localized GFP, membrane- targeted Cyan and cytoplasmic RFP or YFP), generating ten possible distinct colour combinations (Figure 4A). Following injury, SCs of each colour could be observed migrating into the bridge (Figure 4B). Moreover, we found different coloured cells migrating next to each other in the cellular cords (Figure 4C) and these mSC-derived cells were associated with axons in the injury region (Figures 4D and S4A). These results show that previously quiescent mSCs can undergo extensive structural and functional remodelling to become highly migratory cells within a few days of an injury and that they are a polyclonal population. We also observed a significant number of p75+ cells in the migrating cellular cords that were not labelled with a confetti-derived fluorophore (Figure 4B). This suggested that nmSC-derived cells also contributed to the SC population migrating out of the nerve stumps into the bridge.

To confirm that the non-labelled p75+ population were SCs and not the NG2+/PDGFRβ population, we took a number of approaches. Analysis of transverse sections of the bridge region from PLP-eGFP:NG2-dsRed mice found that only 5.14 ± 2.5 % (mean ± SEM, n=4) of the cells in the bridge were NG2+/p75+/eGFP-. Moreover, longitudinal sections of the bridge region showed that these cells were not present within the migrating cell cords (Figure S4C). In addition, analysis of transverse sections of the bridge region from P0-Cre:tdTomato mice (in which all SCs are labelled with tdTomato) found that the vast majority of p75+ within the bridge are also tdTomato positive (95.2 ± 2.1% (mean ± SEM, n=6)). Together these results demonstrate that the migratory population are derived from a combination of nmSCs and mSCs. To determine the proportion of mSCs versus nmSCs, we compared the percentage of recombined SCs in the uncut contralateral nerve of individual P0-CreER^{T2}:tdTomato mice (Madisen et al., 2010) compared to those migrating in the bridge region of the injured nerve. >80% of mSCs were tdTomato+ in the uninjured nerve (Figure S4B), yet in 3 out of 4 mice analysed, the proportion of recombined SCs was lower in the bridge compared to the contralateral uncut nerve (Figure 4E and S4D).. These results suggest that both nmSC and

mSC-derived cells migrate into the bridge following injury but that nmSC-derived cells tend to make a greater contribution to this process.

A second role for SCs during the regenerative response is to contribute to the clearance of the axonal and myelin debris that accumulates in the distal stump, as the axons degenerate and mSCs dedifferentiate following a transection injury (Brosius Lutz et al., 2017; Fernandez-Valle et al., 1995; Gomez-Sanchez et al., 2015). Using P0-CreER^{T2}:tdTomato mice, we could visualise mSC-derived cells that had engulfed myelin debris in the distal stump of injured nerves (Figure S4E), consistent with previous studies suggesting that cells derived from mSCs are able to clear the debris in injured nerves (Brosius Lutz et al., 2017). In contrast p75+/tdTomato- cells do not appear to contain myelin debris probably reflecting that nmSCs do not have access to the myelin debris.

The regenerated nerve has structural abnormalities

It is well established that a regenerated nerve is distinct from an uninjured nerve. In particular, that there is an increase in the number of axons due to increased axonal sprouting during the regenerative process (Bray and Aguayo, 1974; Fawcett and Keynes, 1990; Friede and Bischhausen, 1980; Gutmann and Sanders, 1943). Using EM and the cell-specific markers characterised above, we performed a detailed analysis of the structure and cell composition of the fully regenerated nerve at 6 months following injury. Consistent with previous studies (Salonen et al., 1988; Zochodne, 2008), we found an increase in the density and number of myelinated axons in regenerated nerves and a decrease in the average size of these axons (Figures 5A-B and S5B-C). We also detected a striking difference in the structure of Remak bundles with a large decrease in the number of axons within individual Remak structures (Figures 5A-B). The regenerated nerves also showed a more than three-fold increase in cell density (Figure 5C). This represented a proportional increase of all cell types within the nerve (Figures 5D-E and S5A-B) indicating interactions between the cell types act to maintain the composition of the tissue with the increased number of nmSCs likely explaining the decreased number of axons within each Remak structure. Importantly, we were able to identify all of the cells within the regenerated nerve (Figure 5E) suggesting that all cell-types retain their identity during the regeneration process.

A striking observation was that in regenerated nerve, the level of matrix was dramatically different compared to an uninjured nerve. Matrix levels increase during an injury/regenerative process (Eming et al., 2017) but we found that the additional matrix was not cleared from the regenerated nerve. There were much higher levels of laminin deposition within the basal lamina around the Schwann cells and blood vessels in regenerated nerve (Figures 6A-B). Moreover, the levels of fibronectin and collagen Type III were considerably higher throughout the regenerated nerve (Figures 6A-B). These findings are consistent with the perceived fibrotic nature of repaired tissue and suggest that whereas many cellular changes and the inflammatory

response associated with a regenerative process successfully resolve, the increased matrix deposition associated with tissue regeneration remains within the tissue.

Myelinating Schwann cells maintain their identity during regeneration but show increased plasticity during tumourigenesis

It has been shown previously that adult SCs retain a level of multipotency (Adameyko et al., 2009; Kaukua et al., 2014; Masaki et al., 2013; Widera et al., 2011). However, these studies were mostly in relatively non-physiological situations and it has been shown for other cell types that the environmental context can influence cell plasticity (Anderson, 2001). In particular, a recent study showed that the reported multipotency of pericytes *in vitro* was not recapitulated when lineage analysis was performed in the animal (Guimaraes-Camboa et al., 2017). To address the plasticity of mSCs, we used lineage analysis to track the fate of mSCs following injury. We then compared the behaviour of normal mSCs following injury to those in a mouse model of NF1 tumourigenesis, in which tumours derive from mSCs (Ribeiro et al., 2013). For the injury studies, we treated either P0-CreER^{T2}:YFP or P0-CreER^{T2}:Confetti mice with tamoxifen, 14 days prior to injury and harvested the injured and contralateral uninjured nerves, 6 months later. Analysis of these nerves showed that the vast majority of the labelled mSCs redifferentiated to mSCs, as shown by their morphology and association with large calibre axons and P0 staining (Figure 7A and Figure S6). Importantly, by pulse-labelling mice with a single dose of EdU, 3 days after the injury, we were able to show that mSCs that dedifferentiated and proliferated shortly after injury, remyelinated normally, as we could detect YFP+/EdU+ mSCs within the regenerated nerve (Figure S6). To determine whether cells derived from mSCs contributed proportionally to the new mSC population in regenerated nerve, we compared the rate of recombination in the contralateral nerves to the distal regenerated nerve in mice with lower recombination rates. We found that the proportions remained the same (Figure 7B) providing strong evidence that an additional stem cell or progenitor population was not contributing to the production of mSCs in the regenerated nerve. In contrast, the percentage of recombined cells was lower in some animals in the region of the cut site (Figure 7B). This is consistent with our findings that in some animals, proportionally fewer mSCs migrated into the bridge region compared to those derived from nmSCs (Figure 4E).

To determine whether cells derived from mSCs retained any plasticity, we initially addressed whether these cells could become nmSCs. We analysed the new tissue of the bridge region, where the loss of the Bands of Büngner may permit greater contact with smaller axons and found several examples of labelled SCs that had redifferentiated to become nmSCs, as shown by their association with small calibre axons in the characteristic structure of a Remak bundle

(Figure 7C). We also found these cells within the distal stump region. To confirm these findings, we performed correlative light and electron microscopy (CLEM) and found multiple examples of labelled Remak bundles in the regenerated nerves (Figures 7D and S7). These findings show definitively that mSCs retain the plasticity to become nmSCs following an injury. Moreover, the finding that there was a decrease in the proportion of labelled cells in the bridge region of the cut (Figure 7B) suggests that SCs derived from nmSCs may make a contribution to the regenerated mSC population in this new tissue. Together these findings indicate that dedifferentiated SCs from both the nmSC and mSC population are able to switch between their respective roles.

In contrast to this limited plasticity, we did not find a single example of a mSC becoming another cell type within the regenerated nerve. These findings suggest, that as has been shown for other cell types, that the reported plasticity of cells is due to the non-physiological environment in which the experiments were performed and that the microenvironment is critical for maintaining cell identity (Guimaraes-Camboa et al., 2017; Snippert and Clevers, 2011). Consistent with this view, we found a different scenario in the tumour mouse model (P0-CreER^{T2}:YFP:Nf1$^{fl/fl}$) in which we found that following an injury, tumours derived from mSCs only develop at the injury site (Ribeiro et al., 2013). Analysis of these nerves showed that whilst cells derived from Nf1$^{-/-}$mSCs mostly redifferentiated into mSCs or became tumour cells, a proportion appeared to become other cell types (Figure 7E). These included a large number of cells that expressed Glut1 and resembled perineurial-like cells within the tumour mass (Figure 7E). Moreover, we found several examples of YFP+ cells that had integrated into the perineurium (Figure 7E). These cells were never seen in control animals or in the distal stump of P0-CreER^{T2}:YFP:Nf1$^{fl/fl}$ animals. These findings demonstrate that Schwann cells retain their identity within the context of a regenerating nerve and exhibit limited plasticity, whereas a tumourigenic genetic change and the microenvironment can synergise to increase the plasticity of these cells.

Discussion

It is becoming increasingly clear that different tissues have distinct mechanisms to maintain themselves in the adult and to repair following an injury (Ge and Fuchs, 2018; Varga and Greten, 2017; Wells and Watt, 2018). In proliferative tissues, the classical model of a defined stem cell population dividing infrequently to produce a transiently amplifying population, which then differentiates to produce the various cells of a tissue has been supplanted by more diverse models. These include stem cells that divide frequently, reserve stem cell compartments, the ability of committed cells to dedifferentiate to form stem cells and separate stem cell compartments that are activated upon injury. Moreover, the mechanism to produce new cells often varies dramatically between the homeostatic, injured and repairing states.

Here, we have systematically characterised the cells that make up the endoneurium of peripheral nerves, although we cannot rule out a failure to detect rare cells that are not labelled by any of our methodologies. We find it is a highly quiescent tissue with most cell types proliferating rarely whereas the main cell type of the nerve, the mSC, does not divide at all in the adult. The stability of this tissue is presumably possible because peripheral nerves once formed and matured tend to retain their structure and their connections. Moreover, peripheral nerves are protected by the BNB, which perhaps contributes to the low turnover rate of cells within this tissue. However, once injured, all cell types within a peripheral nerve are able to re-enter the cell-cycle and do so at very high efficiency, apparently obviating the requirement for any stem cell population to produce new cells for the regenerative process. This switch from a highly quiescent tissue to a highly proliferative tissue - with all cell types contributing to the regenerative response represents a further model of how tissues maintain and repair themselves.

In this study, we have also characterised a new cell type. These cells are NG2+/ PDGFRβ+, the classical markers for pericytes. But while these cells are found loosely associated with blood vessels, they are not found within the basal lamina and are negative for αSMA (unlike all the pericytes detected in peripheral nerve). They are also p75+, a marker for dedifferentiated SCs and nmSCs. However, these cells are S100-, and are not marked in any of our SC-specific lineage-tracing mice or in the PLP-eGFP mice. They also have a unique morphology, with long protrusions spreading throughout the endoneurium, which make apparent contact with the other cell types within the nerve. Because of their extensive endoplasmic reticulum, they have previously been referred to as fibroblasts, however, because of their unique set of markers and distinct morphology, we propose to call them tactocytes (touching cells). They make up a substantial proportion (12.5%) of the cells within a peripheral nerve and future studies are needed to uncover their roles in nerve function.

We have characterised the behaviour of the mSC in most detail, which has been possible because of a highly specific driver for this cell type in adulthood that permits credible lineage analysis. These studies show that the mSC is a truly remarkable cell. We were unable to detect a single proliferating mSC throughout the nerves of multiple animals, which indicates that once formed, these highly specialised cells do not turnover. However, these cells are not post-mitotic. Using lineage analysis, we were able to show that following an injury, close to 100% of mSCs proliferated within a few days of the injury. Moreover, they showed a dramatic change in their behaviour to become the migratory cells that transport regrowing axons across the injury site. The ability of all mSCs to proliferate following an injury would seemingly indicate the lack of need for a further stem cell population to produce new SCs during the regeneration of peripheral nerves. This view is further substantiated by lineage analysis of animals with lower levels of recombination, in which we found a similar proportion of

recombined mSCs in an individual animal's uncut and contralateral regenerated sciatic nerve, showing the original population is not diluted by an influx of stem cells from another source. It could thus either be argued that there is not a stem cell/progenitor population to produce new mSCs in the adult or that all mSCs have the capacity to act as stem/progenitor cells. The latter argument is augmented by studies showing that dedifferentiated SCs have unlimited proliferative capacity (Mathon et al., 2001) and retain the ability to redifferentiate back to a more differentiated cell state.

It is particularly striking that very different mechanisms are used to maintain the myelinating cells of the PNS and CNS. New OLs are produced throughout life. Whilst much of this is thought to be to myelinate new axons and is associated with learning and memory, there also appears to be a higher turnover of mature cells, as axons in the optic nerve are fully myelinated yet appear to turnover throughout adulthood (Young et al., 2013). Why mSCs are more stable than OLs in the optic nerve is not clear, as the environments appear similar in that they are both stable structures and are protected by the BNB and BBB respectively. The mechanisms to produce new myelinating cells are also completely different. There only appears to be a requirement to produce new mSCs following injury, as normally these cells do not turnover in the adult. However, following injury, new cells are produced by the dedifferentiation and proliferation of the mSCs themselves. In contrast, the CNS is populated throughout by a precursor cell type (OPCs), which proliferate throughout adulthood to maintain themselves and differentiate throughout life to produce new OLs (Birey et al., 2017). Why such differences exist can only be speculated upon but is likely to reflect a trade-off between the increased plasticity required by the CNS versus the stability required by the PNS. The presence of a continually proliferating progenitor population whilst allowing a rapid source for new myelination also provides a pool susceptible to tumour development. Consistent with this, malignant tumours are more frequent in the CNS compared to the PNS, which perhaps reflects the presence of a more susceptible proliferating progenitor population.

The lineage-analysis used in this study indicates that during the regenerative process, SCs retain their identity. Studies have suggested that SCs retain multipotency, but similarly to *in vivo* studies in other tissues, it appears that the normal tissue environment restricts plasticity (Anderson, 2001; Guimaraes-Camboa et al., 2017). Whilst retaining a SC identity, we did find that dedifferentiated mSCs were able to become nmSCs, showing that these cells retained the ability to respond to the axonal environment and choose between a myelinating or non-myelinating fate. However, we found that this lineage restriction breaks down in the context of tumourigenesis. This required both a tumourigenic mutation (loss of Nf1) and a conducive microenvironment. However, these findings show that increased plasticity can be induced in the SC lineage, which potentially has implications for the pathology of these tumours.

Peripheral nerves regenerate even following a full transection and functionality can be restored in contrast to the poor regenerative capability of the CNS. However, our studies, and others, show that a regenerated nerve differs markedly from an uninjured nerve (Napoli et al., 2012; Salonen et al., 1988; Zochodne, 2008). This includes a large increase in the cellularity of regenerated nerve. Notably, the relative proportion of all cell types remained the same indicating an unknown homeostatic mechanism exists to ensure the structure of the nerve. However, the major difference appears to be increased matrix levels in regenerated nerve. Matrix deposition is a key aspect of an injury response (Eming et al., 2017), and it is likely that the failure to clear injury-induced matrix contributes to the inability of repaired tissue to return to the uninjured state. Targeting the clearance of accumulated matrix could thus provide a strategy for improving tissue repair.

In summary, we report that peripheral nerve provides a further example of the diverse mechanisms by which tissues maintain themselves and repair following injury. In the adult, peripheral nerve is highly quiescent yet retains function throughout adulthood. But, despite this stability, it has remarkable regenerative properties without the need for a specialised stem cell compartment – instead all the cell-types of the nerve are able to proliferate to contribute to the regeneration of this tissue.

Materials and Methods

Transgenic mice

All animal work was performed in accordance with United Kingdom Home Office legislation. Mice were housed in a temperature and humidity controlled vivarium on a 12-hour light-dark cycle with free access to food and water. Female and male (4 week- to 1 year-old) mice of the following genotypes and strains were used: For lineage tracing of mSCs, P0-CreER^{T2} C57Bl/6 mice (Leone et al., 2003; Ribeiro et al., 2013) were crossed with R26R-YFP (Srinivas et al., 2001), R26R-tdTomato (Madisen et al., 2010) or R26R-Confetti reporter mice (Livet et al., 2007; Snippert et al., 2010) to generate P0-CreER^{T2}:YFP, P0-CreER^{T2}:tdTomato and P0-CreER^{T2}:Confetti mice. To visualise all SCs, P0-Cre mice (Feltri et al., 1999) were crossed with R26R-tdTomato mice to generate P0-Cre:tdTomato and Plp-eGFP transgenic mice (Mallon et al., 2002) were used. NG2-dsRed mice were used to confirm the identity of NG2+ cells (Zhu et al., 2008). To distinguish between NG2+/PDGFRβ+/p75+/aSMA- and dedifferentiated SCs within the nerve bridge, Plp-eGFP mice were crossed with NG2-dsRed mice to generate PLP-eGFP:NG2-dsRed mice.

For studying SC plasticity in a nerve tumour environment, P0-CreER^{T2}:YFP:NF1$^{fl/fl}$ mice were used (Ribeiro et al., 2013). In all studies, both male and female mice were used. Animals were genotyped and identified using earhole punches upon weaning. For further details of transgenic mice used in this study see the supplementary Materials and Methods. For lineage

tracing experiments, Cre-mediated recombination was induced in 4-5 week-old mice by intraperitoneal injection (IP) or oral administration of 2mg of tamoxifen (Sigma-Aldrich Cat#H7904) daily for 5 consecutive days. Tamoxifen was dissolved in sunflower oil (20mg/mL) and filtered through a 0.2µm filter.

Sciatic nerve injury

14 days after tamoxifen administration, mice were anaesthetised with isofluorane under aseptic conditions and the right sciatic nerve was exposed at the sciatic notch. The nerve was fully transected or half-transected, as indicated, and the wound closed with clips. Nerves were then collected at the indicated days for analysis by immunostaining or EM.

EdU administration

To cumulatively label newly generated cells, adult c57bl/6 or PLP-eGFP mice received 0.2mg/ml EdU (ThermoFisher Cat# A10044) in their drinking water 0.2mg/ml for up to 70 days as indicated (Young et al., 2013). The water was changed every 48h. For pulse-labelling experiments, a single EdU injection (2mg of EdU in PBS) was given IP, 3 hours prior to tissue collection. Cell proliferation was determined by measuring EdU incorporation detected using the Click-iT^{TM} EdU kit (Thermo Fisher Cat# C10339) according to the manufacturer's instructions.

Immunofluorescence staining

Sciatic nerves were dissected and fixed for 4 hours in 4% paraformaldehyde (PFA) (TAAB) at room temperature and embedded for cryosectioning. For immunostaining, pre- or post-fixed longitudinal sections of the sciatic nerves were immunostained as detailed in the Supplemental Materials and Methods and analysed using confocal microscopy.

Primary antibodies:

The following primary antibodies were used for immunofluorescence at the indicated dilutions: myelin protein zero, P0 (1/500, Abcam, ab39375), p75 (1/500 Millipore ab1554), S100 (1/1000, Dako Z0311), Iba1 (1/500, Wako 019-19741), CD31 (1/100, BD Biosciences 553370), neurofilament 200kD (1/1000, Abcam ab4680), laminin (1/500, Abcam 11575), collagen III (1/1000, Abcam, ab7778), fibronectin (1/500, Sigma-Aldrich, clone FN-3E2), NG2 (1/500, Millipore ab5320), PDGFRβ (1/500, Abcam, ab32570), αSMA (1/1000, Sigma-Aldrich, C6198), GFP (1/1000, Abcam, ab13970), Glut1 (1/500, Abcam, ab652), F4/80 (1/100, Biorad, MCA497G) , NG2 (1/100, Thermo Fisher, MA5-24247). For further details of primary antibodies used in this study see the Supplementary Materials and Methods.

Confocal microscopy

Confocal images were acquired using an inverted SPE or SP8 confocal microscope (Leica). A multiphoton microscope (Zeiss) was used to image confetti samples. Within each experiment, the same acquisition settings were used, the same volume imaged and the same number of z-stacks acquired. Fiji software (https://imagej.net/Fiji/Downloads) was used to make a projection of the z-stacks. For 3D projections, Imaris software was used (http://www.bitplane.com/imaris)

Transmission electron microscopy

Sciatic nerves were dissected and fixed O/N at 4ºC in 2% glutaraldehyde in 0.2M phosphate buffer. Nerves were then post-fixed in 2% osmium tetroxide for 1.5 hours at 4ºC, and incubated in 2% uranyl acetate for 45 minutes at 4ºC. Nerves were dehydrated in an ethanol series before being incubated with propylene oxide and embedded in epoxy resin. 70nm ultra-thin sections were cut with a diamond knife, collected onto formvar coated slot grids and visualised using a transmission electron microscope (TEM, T12 Tecnai Spirit, FEI) using a Morada camera and iTEM software (Olympus SIS). Semi-thin sections were cut using a diamond Histo knife (Diatome) at 0.2µm, dried and stained with 0.5% toluidine blue in 2% Borax at 75°C for 30 seconds. Dried sections were mounted with DPX (Sigma) and representative images of the entire nerves were acquired using a wide-field microscope (Zeiss Axio Scope.A1).

Correlative light and electron microscopy (CLEM)

Regenerated sciatic nerves from P0-CreER^{T2}:Confetti mice were harvested 3 months following injury and fixed in antigenfix (Diapath) overnight. The following day, nerves were embedded in 2.8% low melting point agarose in PBS. 200µm sections of the embedded nerve were cut in cold PBS using a vibrating microtome. For CLEM analysis, sections were first analysed using a SP8 confocal microscope (Leica) and then processed for electron microscopy. For further details of the CLEM protocol used in this study see the Supplementary Materials and Methods.

Quantification and statistical analysis

For details of the image quantification analysis used in this study see the Supplementary Materials and Methods.

Statistical Analysis

Statistical and graphical data analyses were performed using Prism 7 (GraphPad). For all measurements, three or more biological replicates were used. Information regarding the number of biological replicates “n” used in each experiment is reported in the relevant figure legends. The data are represented as mean values ± standard error of the mean (SEM).

Unpaired two-tailed Student's t test was used for statistical analysis except when ANNOVA is indicated. p value significance indicated by asterisks as follows: $*p < 0.05$, $**p < 0.01$, $***p < 0.001$.

Acknowledgements

We would like to thank UCL Biological Services, David Attwell and Michael Hausser for mice and members of the Lloyd laboratory for helpful discussions.

Competing interests

No competing interests declared

Funding

This work was supported by funding from a programme grant from CRUK (C378), a CRUK PhD studentship awarded to SS, a MS Research Australia / Macquarie Group Foundation Paired Fellowship (17-0223), an Alzheimer's Society UK / BUPA Foundation grant awarded to KMY (22095095), MRC project grant, MR/N009169/1 and MRC funding to the MRC LMCB University Unit at UCL, award code MC_U12266B.

References

Adameyko, I., Lallemend, F., Aquino, J. B., Pereira, J. A., Topilko, P., Muller, T., Fritz, N., Beljajeva, A., Mochii, M., Liste, I., et al. (2009). Schwann cell precursors from nerve innervation are a cellular origin of melanocytes in skin. *Cell* **139**, 366-379.

Amoh, Y., Li, L., Campillo, R., Kawahara, K., Katsuoka, K., Penman, S. and Hoffman, R. M. (2005). Implanted hair follicle stem cells form Schwann cells that support repair of severed peripheral nerves. *Proceedings of the National Academy of Sciences of the United States of America* **102**, 17734-17738.

Anderson, D. J. (2001). Stem cells and pattern formation in the nervous system: the possible versus the actual. *Neuron* **30**, 19-35.

Armulik, A., Genove, G. and Betsholtz, C. (2011). Pericytes: developmental, physiological, and pathological perspectives, problems, and promises. *Developmental cell* **21**, 193-215.

Arthur-Farraj, P. J., Latouche, M., Wilton, D. K., Quintes, S., Chabrol, E., Banerjee, A., Woodhoo, A., Jenkins, B., Rahman, M., Turmaine, M., et al. (2012). c-Jun reprograms Schwann cells of injured nerves to generate a repair cell essential for regeneration. *Neuron* **75**, 633-647.

Askew, K., Li, K., Olmos-Alonso, A., Garcia-Moreno, F., Liang, Y., Richardson, P., Tipton, T., Chapman, M. A., Riecken, K., Beccari, S., et al. (2017). Coupled Proliferation and Apoptosis Maintain the Rapid Turnover of Microglia in the Adult Brain. *Cell reports* **18**, 391-405.

Birey, F., Kokkosis, A. G. and Aguirre, A. (2017). Oligodendroglia-lineage cells in brain plasticity, homeostasis and psychiatric disorders. *Current opinion in neurobiology* **47**, 93-103.

Bray, G. M. and Aguayo, A. J. (1974). Regeneration of peripheral unmyelinated nerves. Fate of the axonal sprouts which develop after injury. *Journal of anatomy* **117**, 517-529.

Brosius Lutz, A., Chung, W. S., Sloan, S. A., Carson, G. A., Zhou, L., Lovelett, E., Posada, S., Zuchero, J. B. and Barres, B. A. (2017). Schwann cells use TAM receptor-mediated phagocytosis in addition to autophagy to clear myelin in a mouse model of nerve

injury. *Proceedings of the National Academy of Sciences of the United States of America* **114**, E8072-E8080.

Cattin, A. L., Burden, J. J., Van Emmenis, L., Mackenzie, F. E., Hoving, J. J., Garcia Calavia, N., Guo, Y., McLaughlin, M., Rosenberg, L. H., Quereda, V., et al. (2015). Macrophage-Induced Blood Vessels Guide Schwann Cell-Mediated Regeneration of Peripheral Nerves. *Cell* **162**, 1127-1139.

Cattin, A. L. and Lloyd, A. C. (2016). The multicellular complexity of peripheral nerve regeneration. *Current opinion in neurobiology* **39**, 38-46.

Chen, Z., Pradhan, S., Liu, C. and Le, L. Q. (2012). Skin-derived precursors as a source of progenitors for cutaneous nerve regeneration. *Stem cells* **30**, 2261-2270.

Dimou, L. and Simons, M. (2017). Diversity of oligodendrocytes and their progenitors. *Current opinion in neurobiology* **47**, 73-79.

Domingues, H. S., Portugal, C. C., Socodato, R. and Relvas, J. B. (2016). Oligodendrocyte, Astrocyte, and Microglia Crosstalk in Myelin Development, Damage, and Repair. *Frontiers in cell and developmental biology* **4**, 71.

Eming, S. A., Wynn, T. A. and Martin, P. (2017). Inflammation and metabolism in tissue repair and regeneration. *Science* **356**, 1026-1030.

Fawcett, J. W. and Keynes, R. J. (1990). Peripheral nerve regeneration. *Annual review of neuroscience* **13**, 43-60.

Feltri, M. L., D'Antonio, M., Quattrini, A., Numerato, R., Arona, M., Previtali, S., Chiu, S. Y., Messing, A. and Wrabetz, L. (1999). A novel P0 glycoprotein transgene activates expression of lacZ in myelin-forming Schwann cells. *The European journal of neuroscience* **11**, 1577-1586.

Fernandez-Valle, C., Bunge, R. P. and Bunge, M. B. (1995). Schwann cells degrade myelin and proliferate in the absence of macrophages: evidence from in vitro studies of Wallerian degeneration. *Journal of neurocytology* **24**, 667-679.

Fontana, X., Hristova, M., Da Costa, C., Patodia, S., Thei, L., Makwana, M., Spencer-Dene, B., Latouche, M., Mirsky, R., Jessen, K. R., et al. (2012). c-Jun in Schwann cells

promotes axonal regeneration and motoneuron survival via paracrine signaling. *The Journal of cell biology* **198**, 127-141.

Friede, R. L. and Bischhausen, R. (1980). The fine structure of stumps of transected nerve fibers in subserial sections. *Journal of the neurological sciences* **44**, 181-203.

Ge, Y. and Fuchs, E. (2018). Stretching the limits: from homeostasis to stem cell plasticity in wound healing and cancer. *Nature reviews. Genetics* **19**, 311-325.

Gomez-Sanchez, J. A., Carty, L., Iruarrizaga-Lejarreta, M., Palomo-Irigoyen, M., Varela-Rey, M., Griffith, M., Hantke, J., Macias-Camara, N., Azkargorta, M., Aurrekoetxea, I., et al. (2015). Schwann cell autophagy, myelinophagy, initiates myelin clearance from injured nerves. *The Journal of cell biology* **210**, 153-168.

Guimaraes-Camboa, N., Cattaneo, P., Sun, Y., Moore-Morris, T., Gu, Y., Dalton, N. D., Rockenstein, E., Masliah, E., Peterson, K. L., Stallcup, W. B., et al. (2017). Pericytes of Multiple Organs Do Not Behave as Mesenchymal Stem Cells In Vivo. *Cell stem cell* **20**, 345-359 e345.

Gutmann, E. and Sanders, F. K. (1943). Recovery of fibre numbers and diameters in the regeneration of peripheral nerves. *The Journal of physiology* **101**, 489-518.

Harty, B. L. and Monk, K. R. (2017). Unwrapping the unappreciated: recent progress in Remak Schwann cell biology. *Current opinion in neurobiology* **47**, 131-137.

Jessen, K. R. and Mirsky, R. (2016). The repair Schwann cell and its function in regenerating nerves. *The Journal of physiology* **594**, 3521-3531.

Jessen, K. R., Mirsky, R. and Lloyd, A. C. (2015). Schwann Cells: Development and Role in Nerve Repair. *Cold Spring Harbor perspectives in biology* **7**, a020487.

Joseph, N. M., Mukouyama, Y. S., Mosher, J. T., Jaegle, M., Crone, S. A., Dormand, E. L., Lee, K. F., Meijer, D., Anderson, D. J. and Morrison, S. J. (2004). Neural crest stem cells undergo multilineage differentiation in developing peripheral nerves to generate endoneurial fibroblasts in addition to Schwann cells. *Development* **131**, 5599-5612.

Kaller, M. S., Lazari, A., Blanco-Duque, C., Sampaio-Baptista, C. and Johansen-Berg, H. (2017). Myelin plasticity and behaviour-connecting the dots. *Current opinion in neurobiology* **47**, 86-92.

Kang, S. H., Fukaya, M., Yang, J. K., Rothstein, J. D. and Bergles, D. E. (2010). NG2+ CNS glial progenitors remain committed to the oligodendrocyte lineage in postnatal life and following neurodegeneration. *Neuron* **68**, 668-681.

Kaukua, N., Shahidi, M. K., Konstantinidou, C., Dyachuk, V., Kaucka, M., Furlan, A., An, Z., Wang, L., Hultman, I., Ahrlund-Richter, L., et al. (2014). Glial origin of mesenchymal stem cells in a tooth model system. *Nature* **513**, 551-554.

Leone, D. P., Genoud, S., Atanasoski, S., Grausenburger, R., Berger, P., Metzger, D., Macklin, W. B., Chambon, P. and Suter, U. (2003). Tamoxifen-inducible glia-specific Cre mice for somatic mutagenesis in oligodendrocytes and Schwann cells. *Molecular and cellular neurosciences* **22**, 430-440.

Livet, J., Weissman, T. A., Kang, H., Draft, R. W., Lu, J., Bennis, R. A., Sanes, J. R. and Lichtman, J. W. (2007). Transgenic strategies for combinatorial expression of fluorescent proteins in the nervous system. *Nature* **450**, 56-62.

Madisen, L., Zwingman, T. A., Sunkin, S. M., Oh, S. W., Zariwala, H. A., Gu, H., Ng, L. L., Palmiter, R. D., Hawrylycz, M. J., Jones, A. R., et al. (2010). A robust and high-throughput Cre reporting and characterization system for the whole mouse brain. *Nature neuroscience* **13**, 133-140.

Mahar, M. and Cavalli, V. (2018). Intrinsic mechanisms of neuronal axon regeneration. *Nature reviews. Neuroscience* **19**, 323-337.

Mallon, B. S., Shick, H. E., Kidd, G. J. and Macklin, W. B. (2002). Proteolipid promoter activity distinguishes two populations of NG2-positive cells throughout neonatal cortical development. *The Journal of neuroscience : the official journal of the Society for Neuroscience* **22**, 876-885.

Masaki, T., Qu, J., Cholewa-Waclaw, J., Burr, K., Raaum, R. and Rambukkana, A. (2013). Reprogramming adult Schwann cells to stem cell-like cells by leprosy bacilli promotes dissemination of infection. *Cell* **152**, 51-67.

Mathon, N. F., Malcolm, D. S., Harrisingh, M. C., Cheng, L. and Lloyd, A. C. (2001). Lack of replicative senescence in normal rodent glia. *Science* **291**, 872-875.

McKenzie, I. A., Biernaskie, J., Toma, J. G., Midha, R. and Miller, F. D. (2006). Skin-derived precursors generate myelinating Schwann cells for the injured and dysmyelinated nervous system. *The Journal of neuroscience : the official journal of the Society for Neuroscience* **26**, 6651-6660.

McKenzie, I. A., Ohayon, D., Li, H., de Faria, J. P., Emery, B., Tohyama, K. and Richardson, W. D. (2014). Motor skill learning requires active central myelination. *Science* **346**, 318-322.

Monk, K. R., Feltri, M. L. and Taveggia, C. (2015). New insights on Schwann cell development. *Glia* **63**, 1376-1393.

Napoli, I., Noon, L. A., Ribeiro, S., Kerai, A. P., Parrinello, S., Rosenberg, L. H., Collins, M. J., Harrisingh, M. C., White, I. J., Woodhoo, A., et al. (2012). A central role for the ERK-signaling pathway in controlling Schwann cell plasticity and peripheral nerve regeneration in vivo. *Neuron* **73**, 729-742.

Parrinello, S., Napoli, I., Ribeiro, S., Wingfield Digby, P., Fedorova, M., Parkinson, D. B., Doddrell, R. D., Nakayama, M., Adams, R. H. and Lloyd, A. C. (2010). EphB signaling directs peripheral nerve regeneration through Sox2-dependent Schwann cell sorting. *Cell* **143**, 145-155.

Petersen, J. and Adameyko, I. (2017). Nerve-associated neural crest: peripheral glial cells generate multiple fates in the body. *Current opinion in genetics & development* **45**, 10-14.

Ribeiro, S., Napoli, I., White, I. J., Parrinello, S., Flanagan, A. M., Suter, U., Parada, L. F. and Lloyd, A. C. (2013). Injury signals cooperate with Nf1 loss to relieve the tumor-suppressive environment of adult peripheral nerve. *Cell reports* **5**, 126-136.

Salonen, V., Aho, H., Roytta, M. and Peltonen, J. (1988). Quantitation of Schwann cells and endoneurial fibroblast-like cells after experimental nerve trauma. *Acta neuropathologica* **75**, 331-336.

Snippert, H. J. and Clevers, H. (2011). Tracking adult stem cells. *EMBO reports* **12**, 113-122.

Snippert, H. J., van der Flier, L. G., Sato, T., van Es, J. H., van den Born, M., Kroon-Veenboer, C., Barker, N., Klein, A. M., van Rheenen, J., Simons, B. D., et al. (2010). Intestinal crypt homeostasis results from neutral competition between symmetrically dividing Lgr5 stem cells. *Cell* **143**, 134-144.

Srinivas, S., Watanabe, T., Lin, C. S., William, C. M., Tanabe, Y., Jessell, T. M. and Costantini, F. (2001). Cre reporter strains produced by targeted insertion of EYFP and ECFP into the ROSA26 locus. *BMC developmental biology* **1**, 4.

Tay, T. L., Mai, D., Dautzenberg, J., Fernandez-Klett, F., Lin, G., Sagar, Datta, M., Drougard, A., Stempfl, T., Ardura-Fabregat, A., et al. (2017). A new fate mapping system reveals context-dependent random or clonal expansion of microglia. *Nature neuroscience* **20**, 793-803.

Varga, J. and Greten, F. R. (2017). Cell plasticity in epithelial homeostasis and tumorigenesis. *Nature cell biology* **19**, 1133-1141.

Wells, J. M. and Watt, F. M. (2018). Diverse mechanisms for endogenous regeneration and repair in mammalian organs. *Nature* **557**, 322-328.

Widera, D., Heimann, P., Zander, C., Imielski, Y., Heidbreder, M., Heilemann, M., Kaltschmidt, C. and Kaltschmidt, B. (2011). Schwann cells can be reprogrammed to multipotency by culture. *Stem cells and development* **20**, 2053-2064.

Young, K. M., Psachoulia, K., Tripathi, R. B., Dunn, S. J., Cossell, L., Attwell, D., Tohyama, K. and Richardson, W. D. (2013). Oligodendrocyte dynamics in the healthy adult CNS: evidence for myelin remodeling. *Neuron* **77**, 873-885.

Zhu, X., Bergles, D. E. and Nishiyama, A. (2008). NG2 cells generate both oligodendrocytes and gray matter astrocytes. *Development* **135**, 145-157.

Zochodne, D. W. (2008). Neurobiology of Peripheral Nerve Regeneration. *Cambridge University Press*

Zochodne, D. W. (2012). The challenges and beauty of peripheral nerve regrowth. *Journal of the peripheral nervous system : JPNS* **17**, 1-18.

Figures

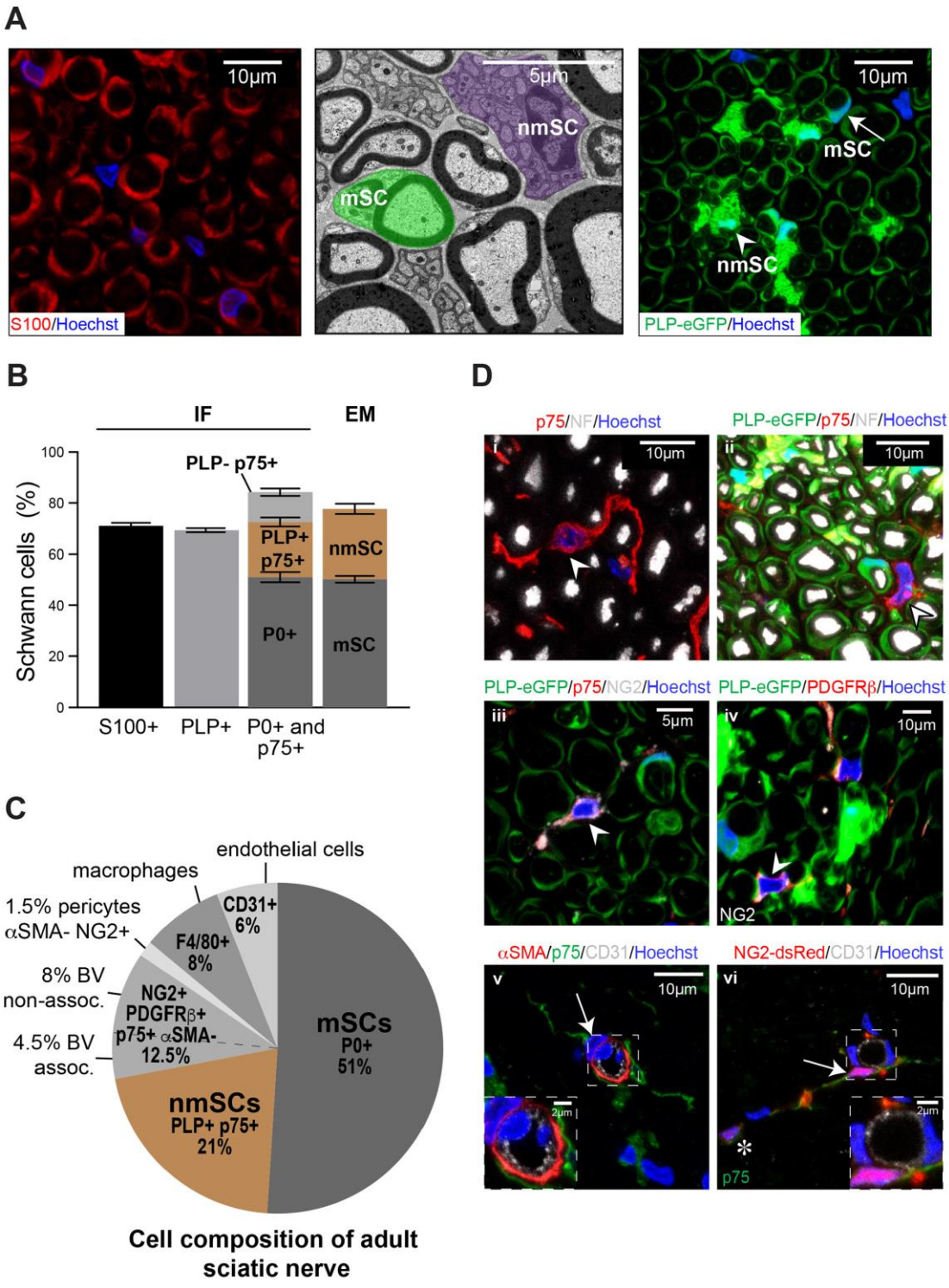

Figure 1: Identification of the cell composition of peripheral nerve

A) Representative confocal immunofluorescence (IF) and EM images showing the SC population in transverse sections of mouse sciatic nerve. SCs are labelled either by staining with a S100 antibody (red) or endogenously using PLP-eGFP mice (green). In the EM image, a nmSC is coloured purple while a typical mSC is coloured green. **B)** Quantification shows the proportion of Schwann cells in mouse sciatic nerve (n=4 mice, mean ±SEM). **C)** Pie chart showing the percentage of individual cell types within sciatic nerve. Cryosections of sciatic nerves were immunolabelled with cell type specific markers as indicated (n=4). The NG2+/PDGFRβ+/αSMA- population is classified as either associated or non-associated with CD31+ blood vessels (BV). Pericytes are defined as NG2+/PDGFRβ+/αSMA+. **(D)** Representative images of transverse mouse sciatic nerve sections labelled as indicated. (i) Arrowhead indicates a p75+ cell (red) that is not associated with axons (white) (ii) Arrowhead indicates a p75+ cell (red) that is not associated with axons (white) and does not express eGFP in nerves isolated from PLP-eGFP mice. (iii) Arrowhead indicates a PLP-eGFP-/p75+/NG2+ positive cell (iv) Arrowhead indicates a PLP-eGFP-/NG2+/ PDGFRβ+ positive cell. (v) Arrow indicates a αSMA+/p75- pericyte in close contact with a CD31+ blood vessel (white). (vi) Arrow indicates a p75+ cell that co-expresses dsRed in nerves isolated from NG2-dsRed mice and is loosely associated with a CD31+ blood vessel. The asterisk indicates a p75+/dsRed+ cell that is not associated with a blood vessel. (v+vi) Dashed white boxes indicate the regions that are shown at higher magnification. See also Figure S1.

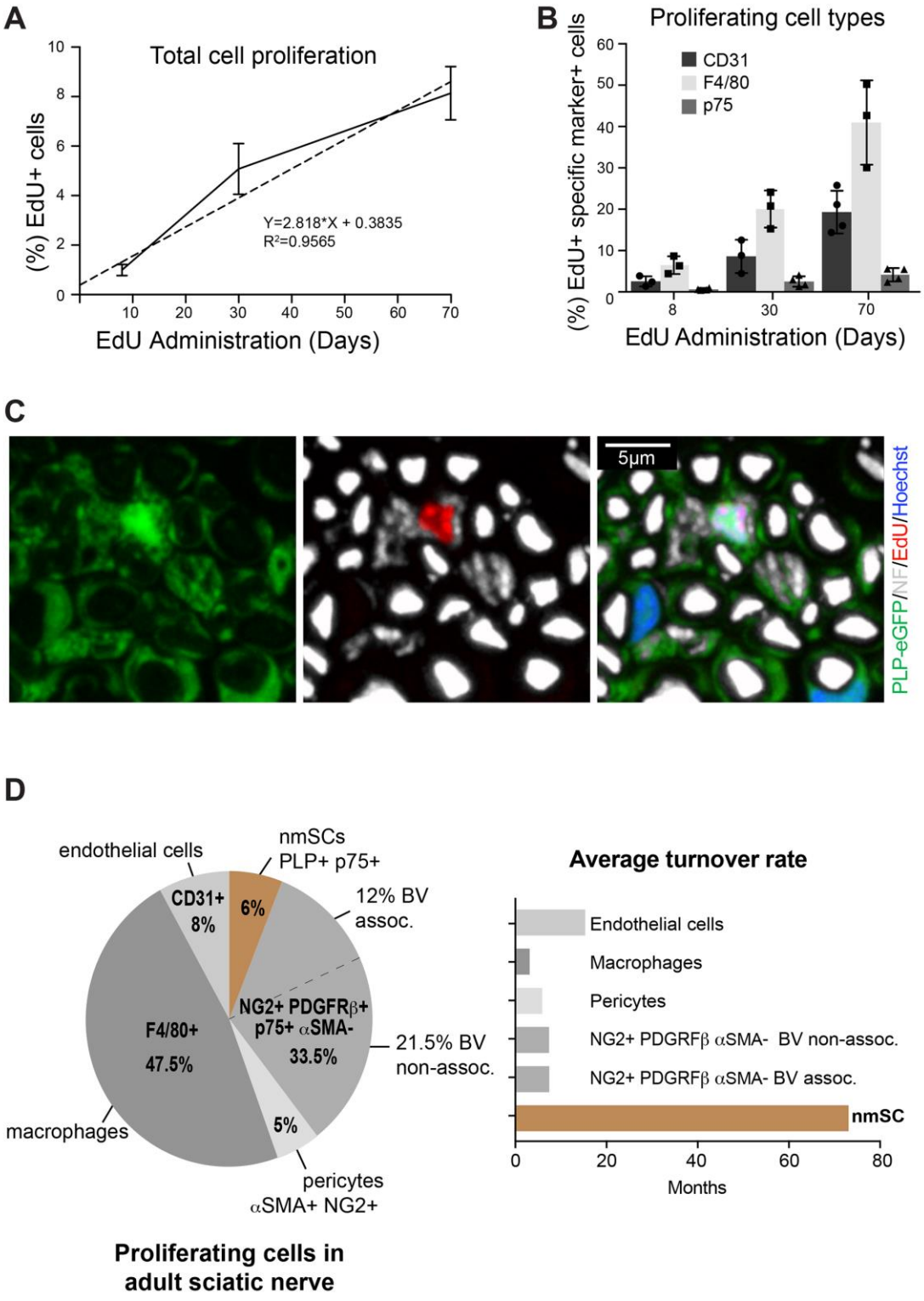

Figure 2: Peripheral nerve is a highly quiescent tissue.

A) EdU was administered continuously in the drinking water of WT mice for 8, 30 and 70 days. Cryosections of sciatic nerve were processed to detect EdU. Graph shows the mean percentage (±SEM) of EdU+ cells that accumulate over time (n=3-4 mice). **B)** Cryosections of sciatic nerves were labelled with cell specific markers and processed to detect EdU+ cells. (n=3-4 mice, ±SEM). **C)** 3D projection of a confocal image of a 20μm cryosection of sciatic nerve isolated from a PLP-eGFP mouse treated with EdU continuously for 30 days, showing a EdU+ (red), non-myelinating Schwann cell (eGFP+) associated with small axons (white). **D)** Pie chart showing the proportion of proliferating cell types in adult sciatic nerve in mice treated with EdU for 30 days (n=6 mice). Graph shows the calculated turnover time for each cell population. See also Figure S2 and Movie S1.

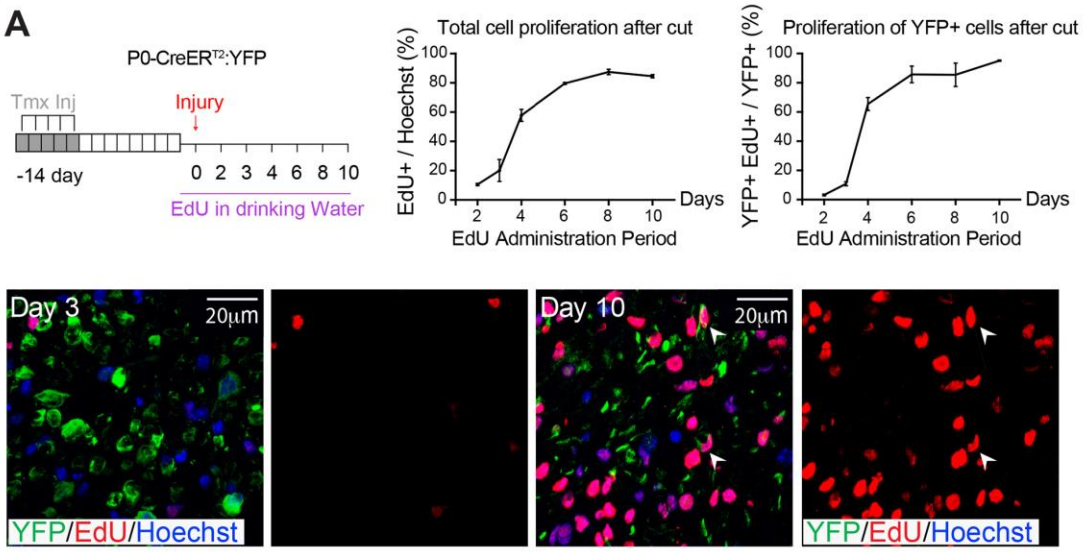

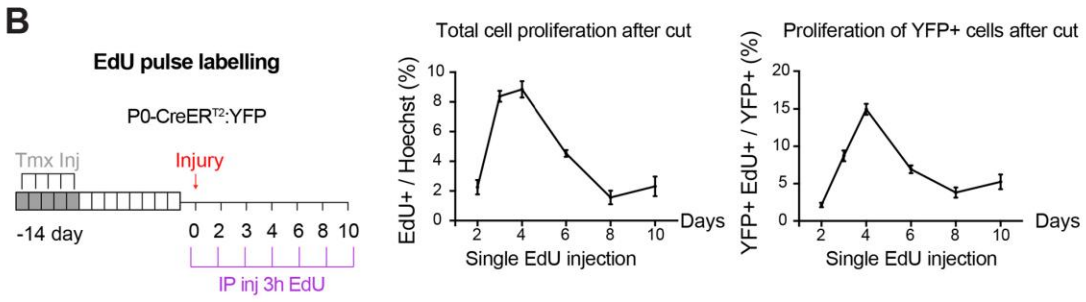

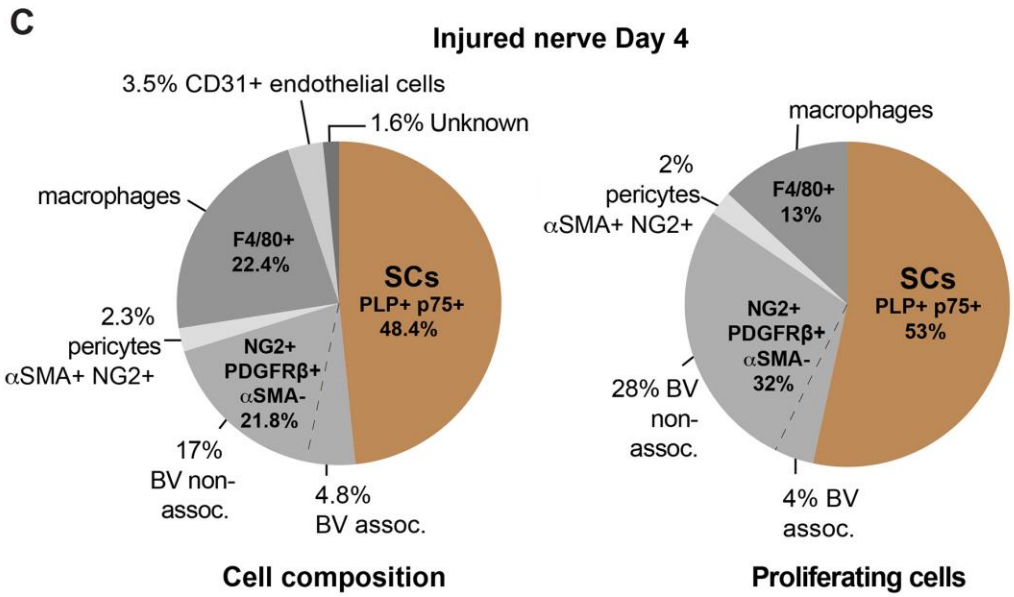

Figure 3: **All mSCs proliferate following injury.**

A) Schematic showing the protocol to assess accumulated proliferation of mSCs following injury. P0-CreER^{T2}:YFP mice were treated with tamoxifen (Tmx) for five days to specifically label mSCs with YFP. Fourteen days later, the right sciatic nerve was transected and EdU was administered continuously in the drinking water for ten days. Mice were harvested at the indicated time points and proliferating (EdU+) cells were counted in cryosections of the distal stump (downstream of the newly-formed bridge region) of sciatic nerve processed for IF staining. Graphs show the percentage of proliferating cells (EdU+/Hoechst) or the percentage of proliferating mSCs (YFP+, EdU+/YFP+) plotted against the time of EdU administration (n=4 mice, ±SEM). Representative images show few mSCs have proliferated at Day 3 following injury. In contrast, almost all mSCs have proliferated at Day 10 post-injury. Arrowheads indicate proliferating mSCs. **B)** Schematic showing the protocol used to perform a temporal analysis of the proliferation of mSCs following injury. Mice were treated as in **(A)** but the EdU was administered by IP, 3 hours prior to the culling of the animals at the indicated times. Graphs show the percentage of all proliferating cells (EdU+/Hoechst) or the percentage of proliferating mSCs (YFP+, EdU+/YFP+) at the indicated time points (n=4-6 mice, ±SEM). **C)** Pie charts show the cell composition and relative contribution of each cell type to the proliferating population in the distal stump of an injured sciatic nerve on Day 4 following injury, which is the peak time of proliferation (n=8 mice). See also Figure S3.

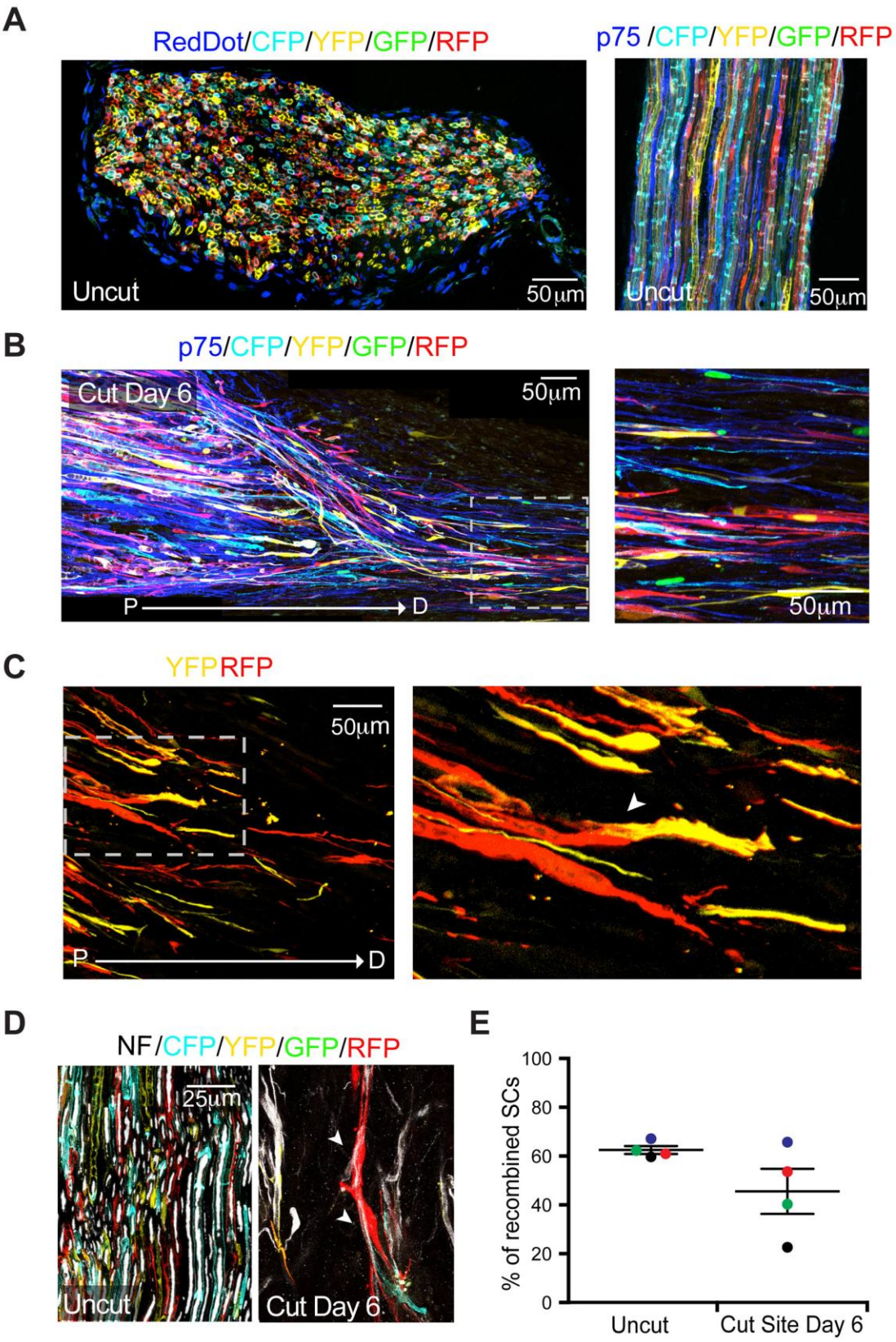

Figure 4: mSCs become migratory following injury to guide regrowing axons across the injury site.

A) Representative images of transverse (left panel) and longitudinal (right panel) cryosections of uninjured contralateral sciatic nerve showing the high recombination rate in P0-CreER^{T2}:Confetti mice following tamoxifen administration. Nuclei were labelled with RedDot (left panel) and p75 antibody was used to label non-myelinating SCs (right panel). **B)** Representative longitudinal cryosection (left panel) and a higher magnification (right panel) of a transected sciatic nerve showing that cells derived from mSCs have migrated into the nerve bridge, at Day 6 following nerve injury. An antibody to p75 was used to label dedifferentiated SCs. **C)** Representative longitudinal cryosection (left panel) and higher magnification (right panel) of the bridge of a transected sciatic nerve. Arrowhead indicates a cord of two migrating SCs that have derived from different mSCs (YFP+ and RFP+). **D)** Representative images of longitudinal sections of an uninjured and transected sciatic nerve, Day 6 following injury shows that dedifferentiated SCs derived from mSCs associate with axons while migrating into the nerve bridge. An antibody to neurofilament (NF) was used to label the axons (white). Arrowheads indicate migrating SCs associated with axons. **E)** Graph shows the percentage of recombined SCs (tdTomato/(mSCs + nmSCs)) in the bridge of the injured sciatic nerve of P0-CreER^{T2}:tdTomato mice, Day 6 after injury and in the contralateral uninjured sciatic nerve (uncut). Each coloured dot represents an individual animal. Line shows mean±SEM. See also Figure S4.

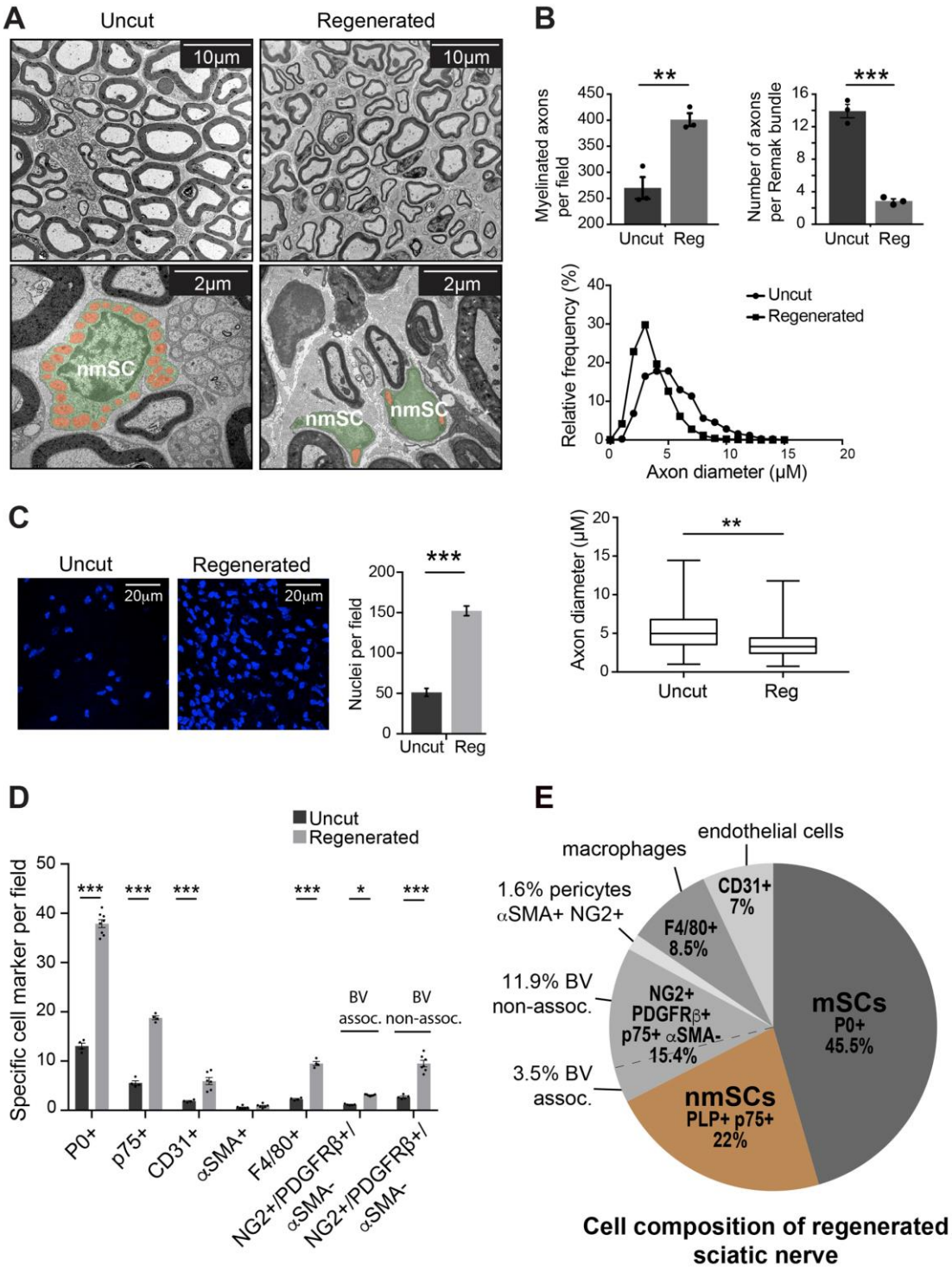

Figure 5: Regenerated nerve is distinct from uninjured nerve.

A) Representative EM images of uncut contralateral or regenerated nerve taken 6 months following injury. Note that the regenerated nerve has smaller axons and more myelinated axons per field in contrast to the uncut nerve. The lower panels show a higher magnification of the EM images in which nmSCs are highlighted in green and small calibre axons in orange to show the decreased numbers of axons per Remak bundle in the regenerated nerve. **B)** Graphs show the quantification of **(A)** to show the density of myelinated axons, the number of axons per Remak bundle (n=3 mice, mean±SEM) and the axon diameters (n=8 mice) in uncut and regenerated nerve. **C)** Representative confocal images of transverse sections of uninjured and regenerated sciatic nerve, 6 months after injury, showing Hoechst+ cells (blue). Graph shows the quantification of the number of nuclei per field. (n=8 mice, mean±SEM). **D)** Cryosections of regenerated and uninjured sciatic nerve were immunolabelled for cell type specific markers as indicated, 6 months following injury and the number of the different cell types was quantified per field. (n=4-8 mice, mean±SEM, two-way ANNOVA was used). **E)** Pie chart shows the cell composition of regenerated sciatic nerve, 6 months following injury (n=4-8 mice). See also Figure S5.

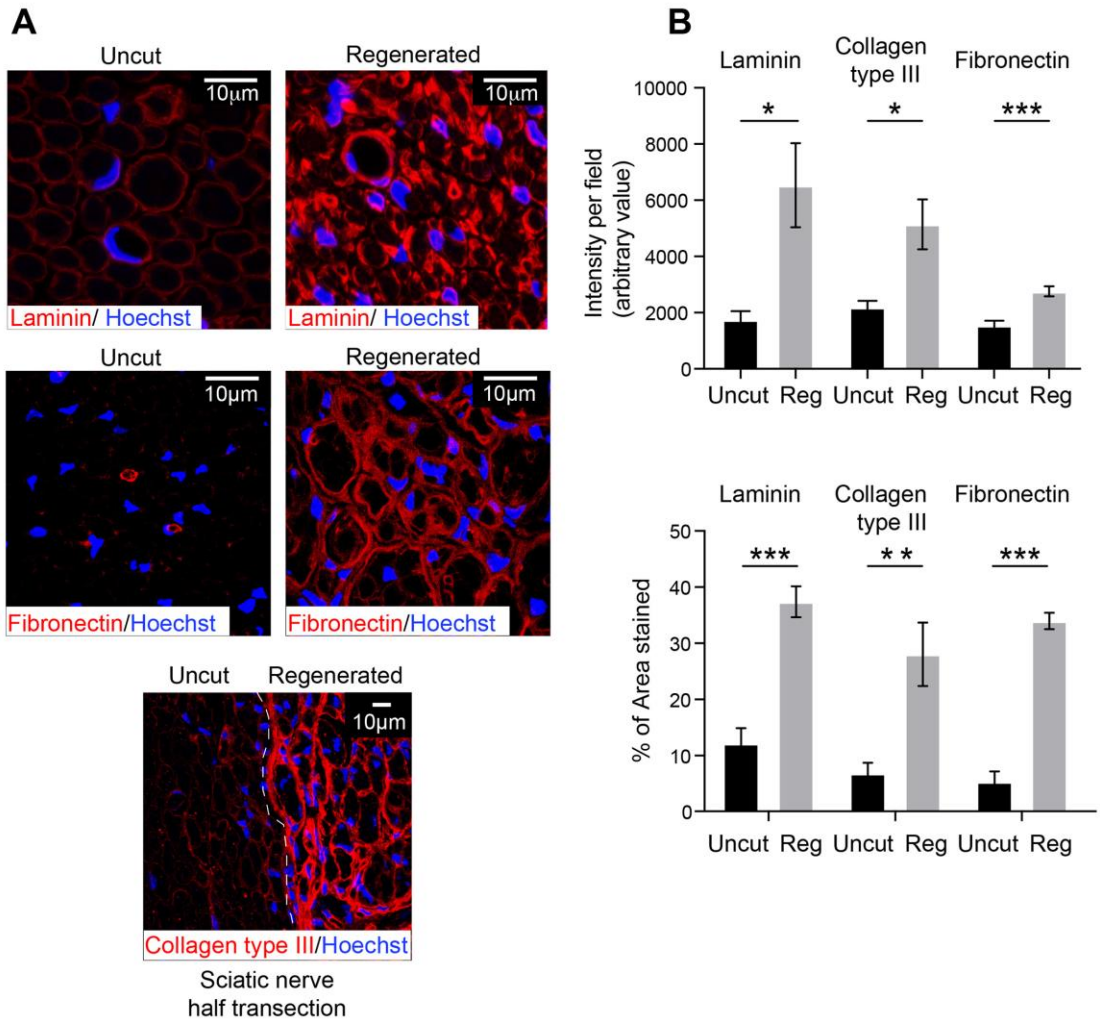

Figure 6: The levels of ECM proteins remain high in regenerated nerve.

A) Representative confocal images of transverse sections of uninjured and the distal stump of regenerated sciatic nerve, 6 months following injury, immunostained for the indicated ECM proteins. **B)** Graphs show quantification of **(A)** (n=6 mice, mean±SEM).

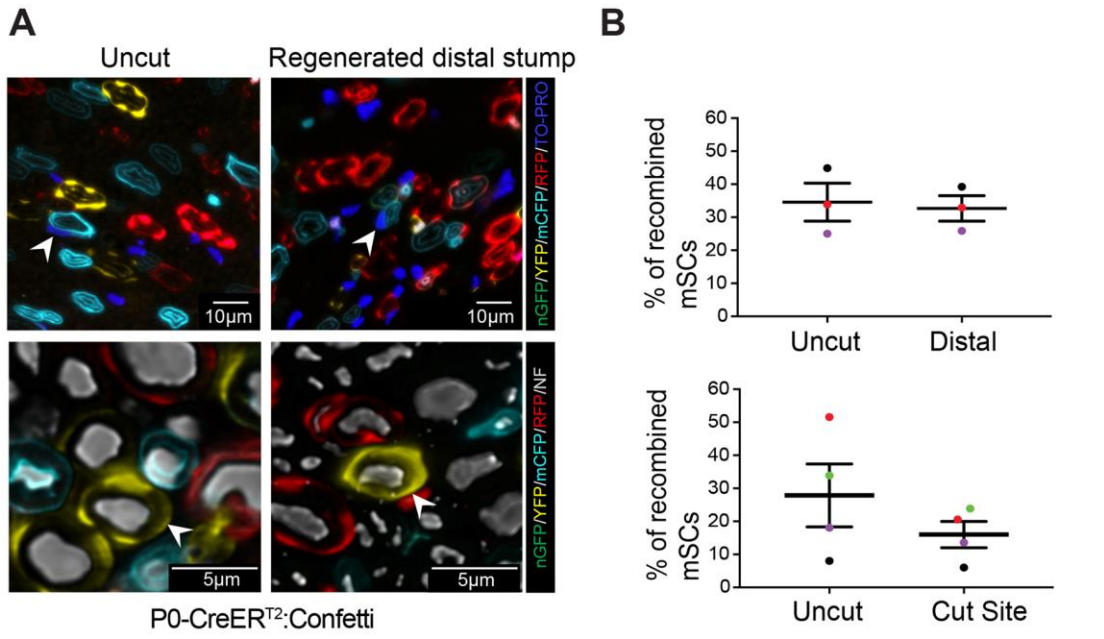

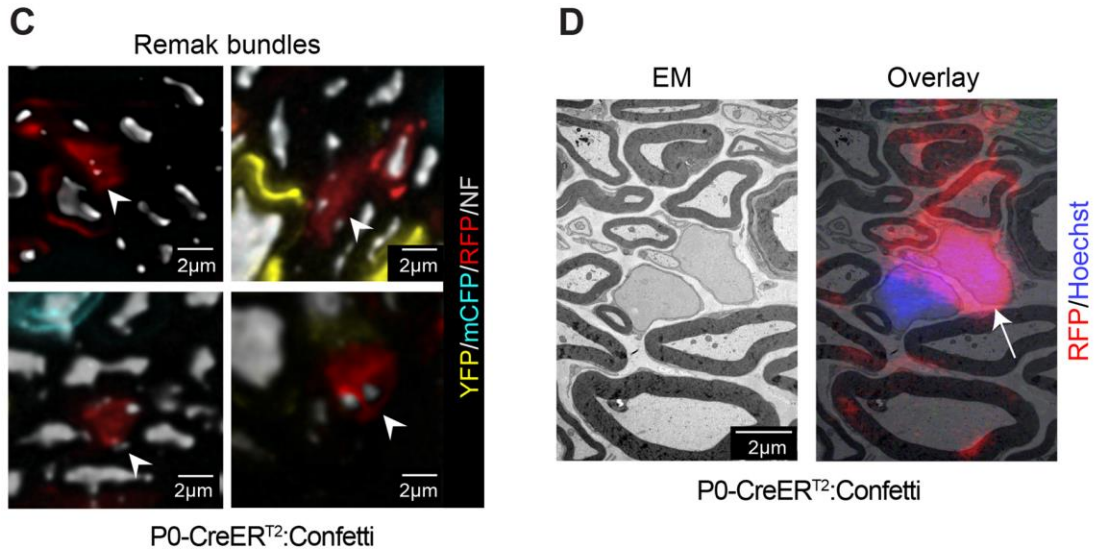

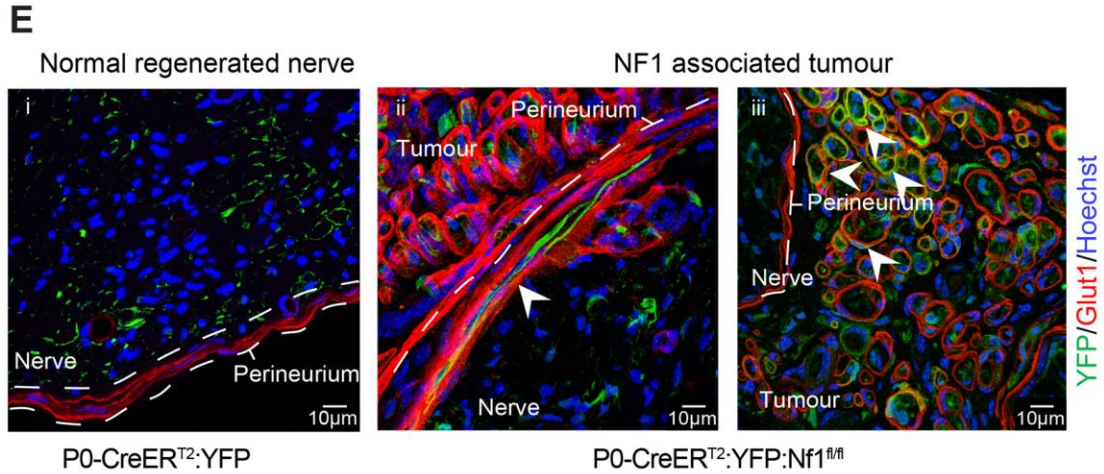

Figure 7: mSCs retain a SC fate following nerve injury but can switch to become a nmSC.

A) Representative confocal images of uncut and the regenerated distal stump of P0-CreER^{T2}:Confetti mice, 6 months following injury. The majority of the labelled mSCs redifferentiated back to mSC, as seen by their morphology and association with large calibre axons, labelled for neurofilament (white). Arrowheads indicate examples. Nuclei are labelled in the upper panel with TO-PRO (dark blue). **B)** Graphs show the percentage of recombined mSCs in the distal stump and at the injury site of P0-CreER^{T2}:Confetti mice, 6 months following injury compared to the uninjured contralateral nerve. Each coloured dot indicates an individual animal. Line shows mean±SEM. **C)** Representative confocal images of transverse sections of regenerated sciatic nerves of P0-CreER^{T2}:Confetti mice showing labelled mSCs, which have redifferentiated into nmSCs. Arrowheads indicate labelled Remak bundles associated with small calibre axons (labelled for neurofilament (NF, white). **D)** CLEM images of a 200µm transverse section of sciatic nerve from a P0-CreER^{T2}:Confetti mouse, Day 90 after nerve transection showing a RFP-labelled mSC (indicated by an arrow) that has redifferentiated to become a nmSC following injury. **E)** Representative confocal images showing (i) a regenerated nerve of P0-CreER^{T2}:YFP mice, in which mSCs retain their lineage and (ii+iii) which show tumours from P0-CreER^{T2}:YFP:Nf1$^{fl/fl}$ mice, which develop neurofibromas derived from NF1$^{-/-}$ mSCs specifically at the injury site. Arrowheads indicate Nf1$^{-/-}$/YFP+ mSC-derived cells, which have taken a different cell fate within the tumour. (ii) shows a YFP-positive cell which has integrated within the perineurium and (iii) shows a number of YFP-positive, perineurial-like cells which have a distinct morphology and are labelled with Glut1, a marker of perineurial cells. See also Figures S6 and S7.

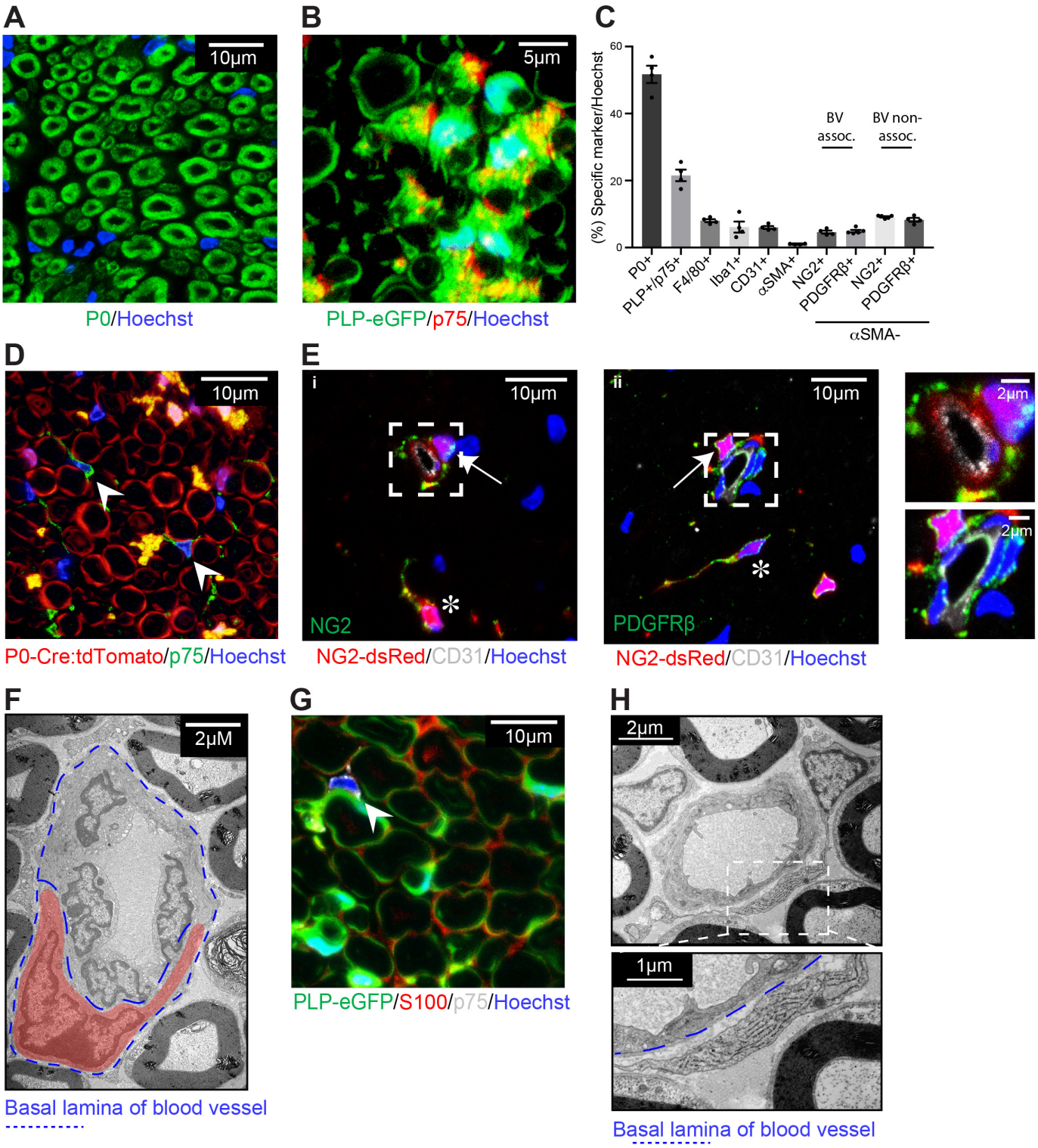

Figure S1, related to Figure 1. Identification of the cell composition of peripheral nerve.
Representative confocal images of **A)** mSCs (P0+) and **B)** nmSCs (PLP+/ p75+). **C)** Graph shows the quantification of specific markers expressed by cells in sciatic nerve (n=4-5 mice, mean±SEM). Pericytes are defined by the co-expression of NG2, PDGFRß and αSMA. A separate population is NG2/ PDGFRß+ but αSMA-. These cells were further characterised as associated or non-associated with CD31+ blood vessels (BV). **D)** Representative confocal image shows a transverse section of a sciatic nerve isolated from a P0-Cre:tdTomato mouse immunostained for p75 (green). Arrowheads indicate tdTomato-/ p75+ cells. **E)** Sections from NG2-dsRed mice were co-stained for (i) NG2 (green) and (ii) PDGFRß (green). Arrows indicate CD31+ - associated cells, asterisks indicate a CD31+ non-associated population. White rectangles indicate the regions that are shown at higher magnifiation on the right. **F)** Representative EM image showing a classical pericyte (red), which is in tight contact with a blood vessel and is within the basal lamina. **G)** Transverse section of a sciatic nerve isolated from a PLP-eGFP mouse immunostained for p75 (grey) and S100 (red). Arrowhead indicates an eGFP-/S100-/p75+ cell. **H)** Representative EM images show an elongated cell, rich in endoplasmic reticulum, closely associated with a blood vessel. The higher magnification image shows that it is not surrounded by the basal lamina.

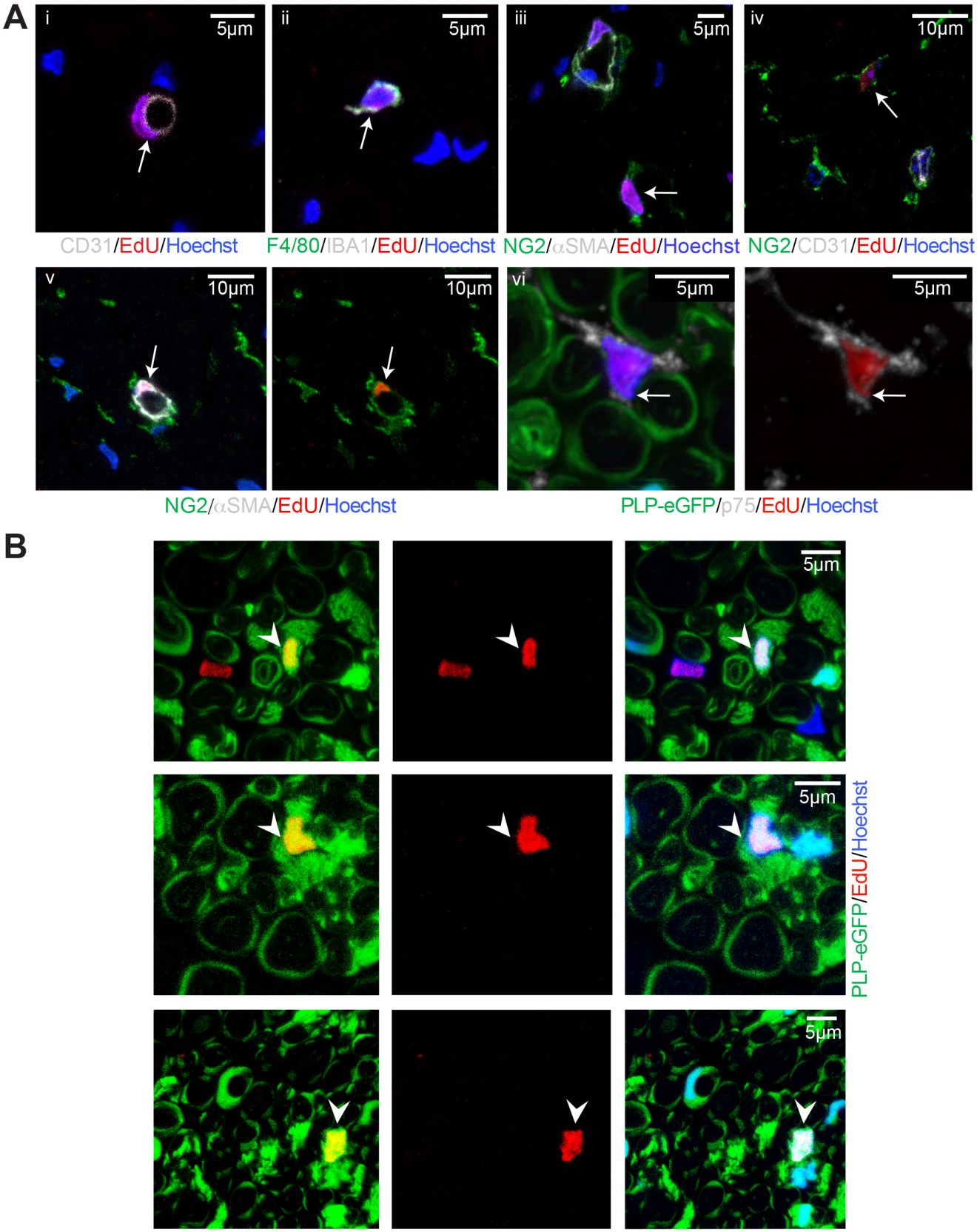

Figure S2, related to Figure 2. Peripheral nerve is a highly quiescent tissue.
A) Representative confocal images of (i-v) transverse sections of sciatic nerve from WT mice and (vi) PLP-eGFP mice treated continuously with EdU for 30 days, processed to detect EdU (red) and immunolabelled for (i) CD31, to detect endothelial cells (white). (ii) F4/80 (green)/ Iba1 (white), to detect macrophages. (iii) NG2 (green) and αSMA (white) to detect pericytes. (iv) NG2 (green), and CD31 (white) to detect NG2+ cells non-associated with CD31+ blood vessels. (v) NG2 (green) and αSMA (white). (vi) p75 (white) to detect PLP-/ p75+/ EdU+ cells. Nuclei are stained with Hoechst (blue). Arrows indicate proliferating cells. **B)** Confocal images of 20μm cryosections of sciatic nerve isolated from PLP-eGFP mice treated continuously with EdU (red) for 30 days. Nuclei are stained with Hoechst (blue). Arrowheads indicate three separate examples of proliferating nmSCs (PLP+/ EdU+).

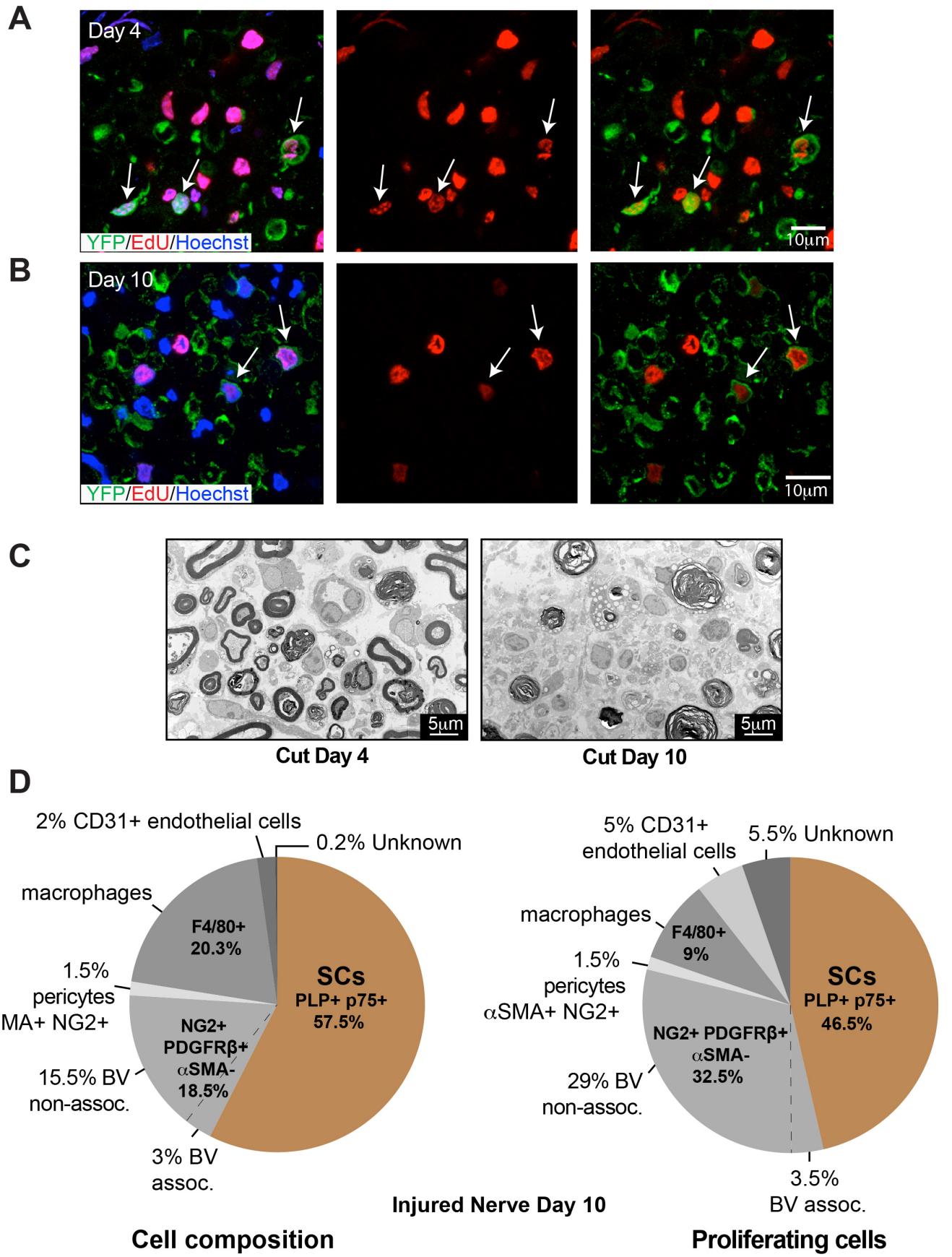

Figure S3, related to Figure 3. All mSCs proliferate following injury.
A-B) Representative confocal images of transverse sections of transected sciatic nerve of P0-CreER^{T2}:YFP mice in which mSCs were labelled with YFP following Tmx administration. Arrows indicate Edu+/ YFP+ cells **A)** Day 10 following injury, EdU was administered continuously in the drinking water. **B)** Day 4 following injury, EdU was injected 3 hours prior to harvesting. **C)** Representative EM images of the distal stump of injured sciatic nerves at Day 4 and Day 10 following transection. **D)** Pie charts show the cell composition and the relative proportions of the cell types proliferating in the distal stump of an injured sciatic nerve at Day 10 following injury (n=8 mice).

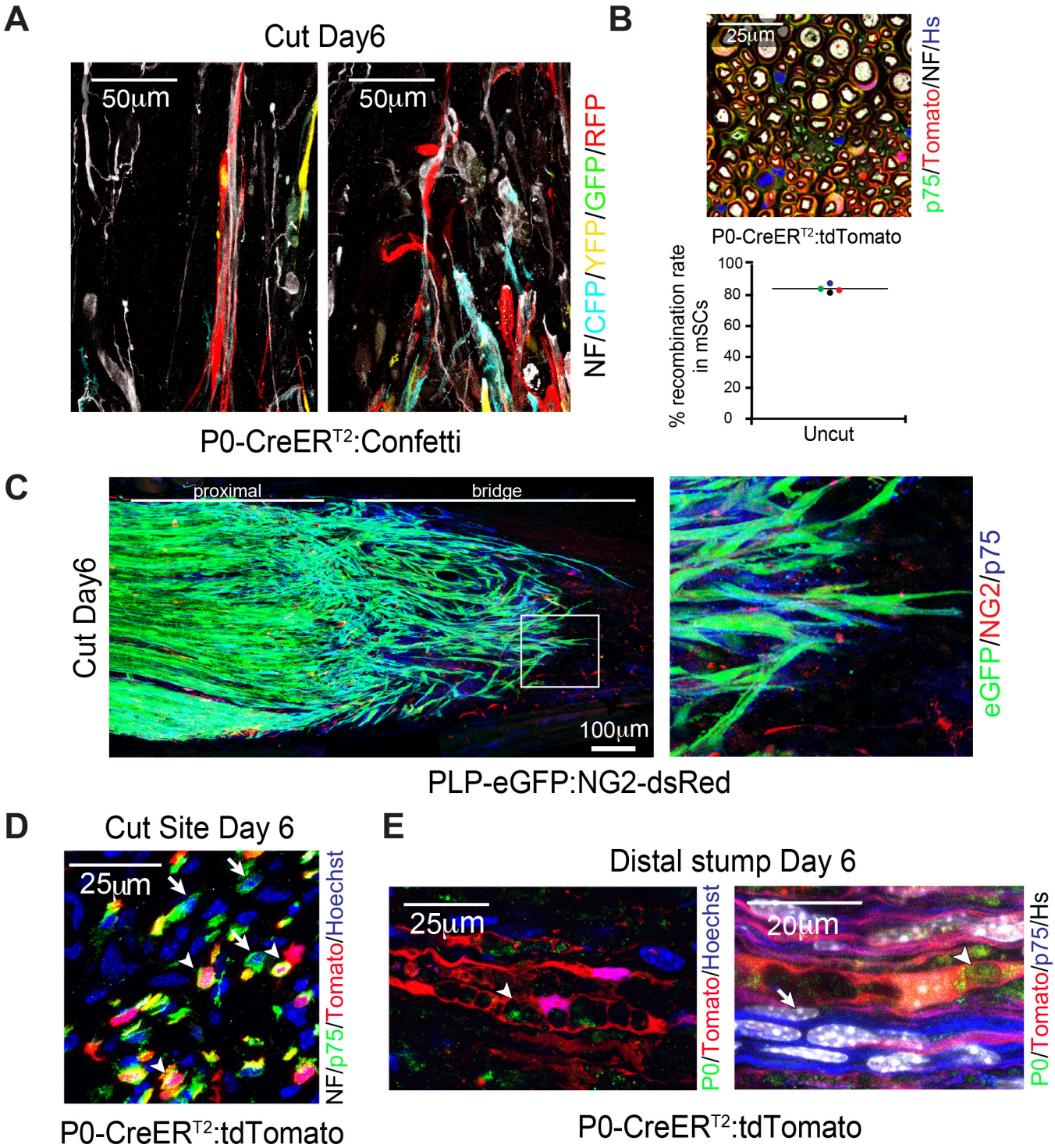

Figure S4, related to Figure 4 : mSCs become migratory following injury to guide regrowing axons.
A) Representative images of a longitudinal cryosection of an injured sciatic nerve of P0-CreER^{T2}:Confetti mice, Day 6 following injury, shows migrating SCs derived from mSCs associated with regrowing axons in the nerve bridge. An antibody to neurofilament (NF) was used to label the axons. **B)** Representative image of a transverse cryosection of uninjured sciatic nerves of P0-CreER^{T2}:tdTomato mice following tamoxifen administration. Antibodies to S100 and neurofilament (NF) were used to label SCs and axons, respectively. Graph shows the percentage of recombined mSCs and shows that more than 80% of mSCs express Tomato following tamoxifen administration. Each coloured dot represents an individual animal. Line shows mean±SEM. **C)** Representative image of a longitudinal cryosection of the bridge region (Cut site) of an injured sciatic nerve from PLP-eGFP:NG2-dsRed mice, Day 6 following injury. An Antibody to p75 was used to label dedifferentiated SCs. **D)** Representative image of a transverse cryosection of the bridge region (Cut site) of an injured sciatic nerve from P0-CreER^{T2}:tdTomato mice, Day 6 following injury. Antibodies to p75 and neurofilament (NF) were used to label dedifferentiated SCs and axons, respectively. Arrowheads indicate Tomato+/p75+ cells and arrows Tomato-/p75+ cells and show that SCs derived from mSCs are associated with axons in the bridge region. **E)** Representative images of a longitudinal section of the distal stump of P0-CreER^{T2}:tdTomato mice, showing that SCs derived from mSCs engulf and degrade myelin debris. Antibodies to P0 and p75 weres used to label dedifferentiated SCs and the degraded myelin, respectively. Arrowheads indicate myelin debris that has been engulfed by myelinating Schwann cell derived cells and the arrow indicates a Tomato-/P75+ cell devoid of myelin debris.

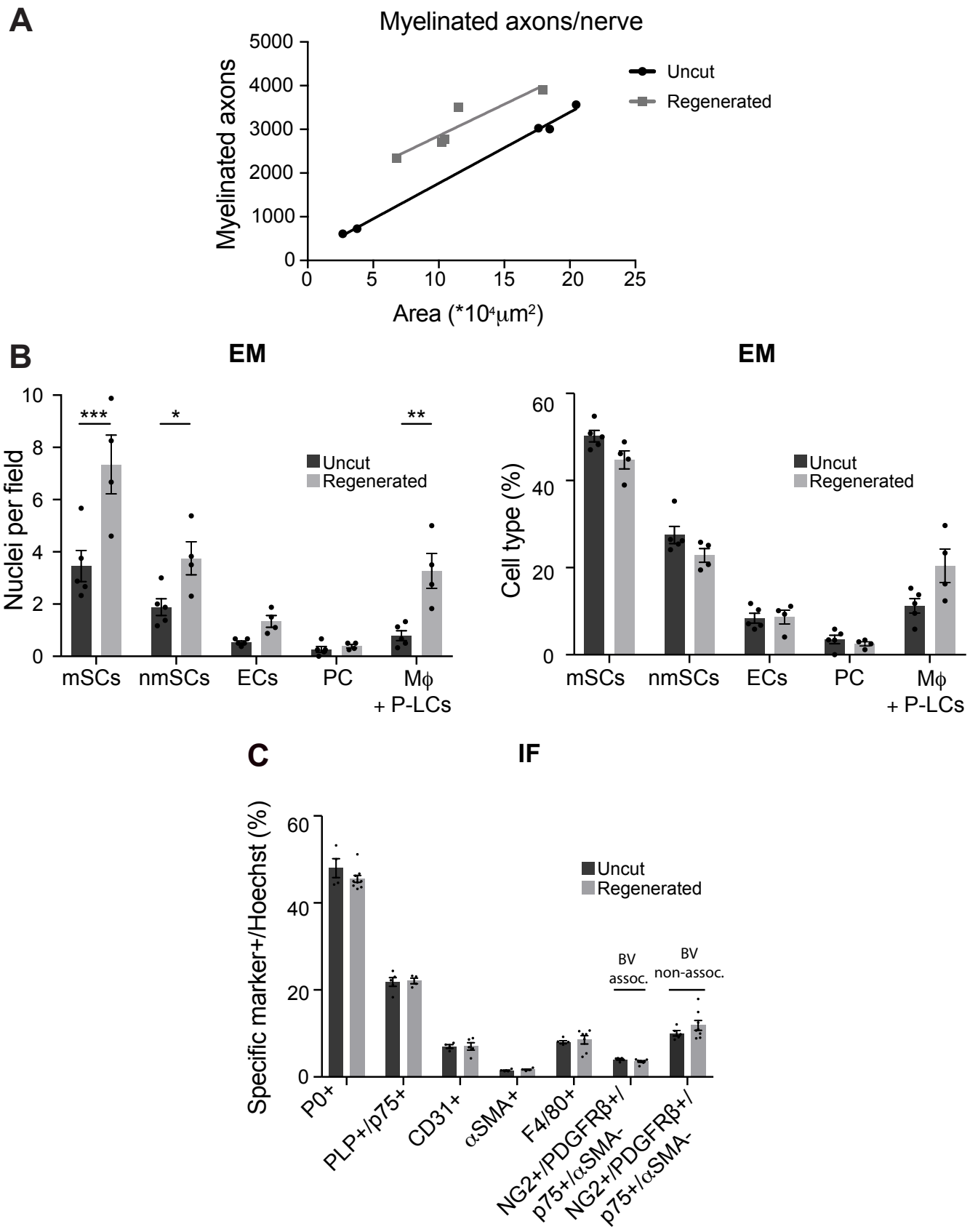

Figure S5, related to Figure 5. Regenerated nerve is distinct from uninjured nerve.
A) Graph shows the quantification of the total number of axons in uncut and regenerated nerve. Each point represents an individual nerve. **B)** Quantification of EM images showing the number of specific cell types per field (LHS) and the proportion of each cell type (RHS) in uncut and regenerated nerves, 6 months following injury. Cells were identified by morphology. EC (endothelial cells), PC (pericytes). We were not confident distinguishing macrophages (Mϕ) from NG2+/ PDGFRβ/ P75+ cells, labelled as P-LCs (pericyte-like cells) in the EM quantifications, and so these cells were grouped together (n=4-5 mice, mean±SEM, two-way ANNOVA was used). **C)** Quantification of immunofluorescent images showing the proportion of each cell type, identified by the indicated markers, in the uncut and regenerated nerves, 6 months following injury (n=4-9 mice, mean±SEM).

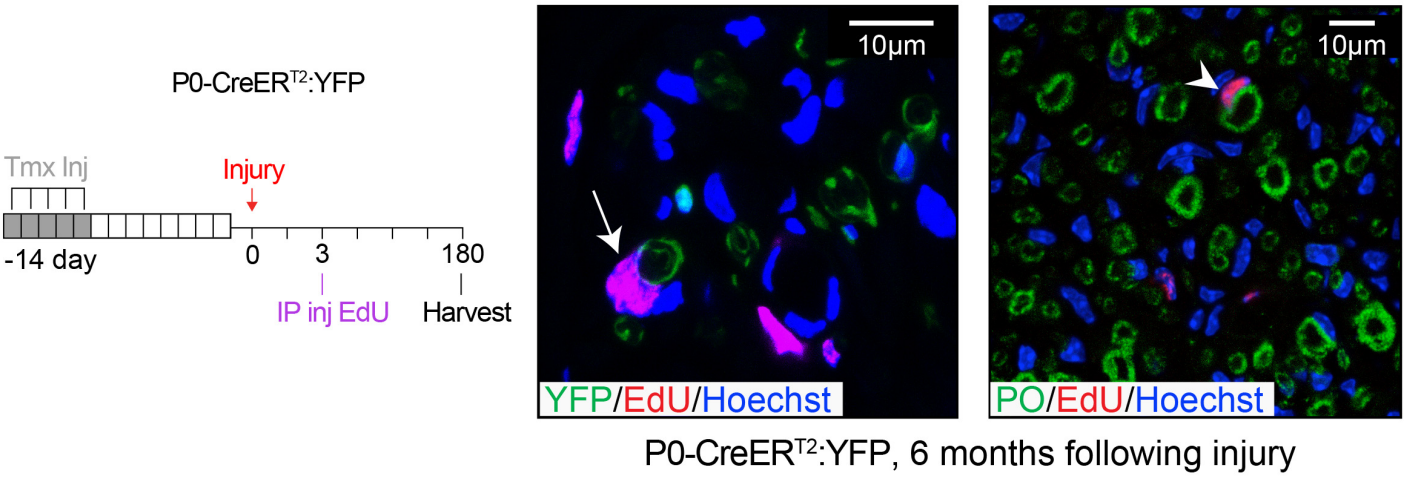

Figure S6, related to Figure 7. mSCs retain a SC fate following nerve injury but can switch to become a nmSC.
Schematic representation of the protocol used to determine whether proliferating cells derived from mSCs remyelinate axons. P0-CreER^{T2}:YFP mice were injected intraperitoneally with Tmx for 5 consecutive days. 14 days following the first injection, the right sciatic nerve was cut and EdU was injected at Day 3 following injury. Mice were harvested 6 months later. Representative confocal images show transverse sections from the regenerated nerve of EdU injected P0-CreER^{T2}:YFP mice, 6 months following injury. The arrow indicates a YFP+ mSC that proliferated at Day 3 following injury and redifferentiated into a mSC. The arrowhead indicates a cell that proliferated at Day 3 following injury and became a mSC, as indicated by P0 staining.

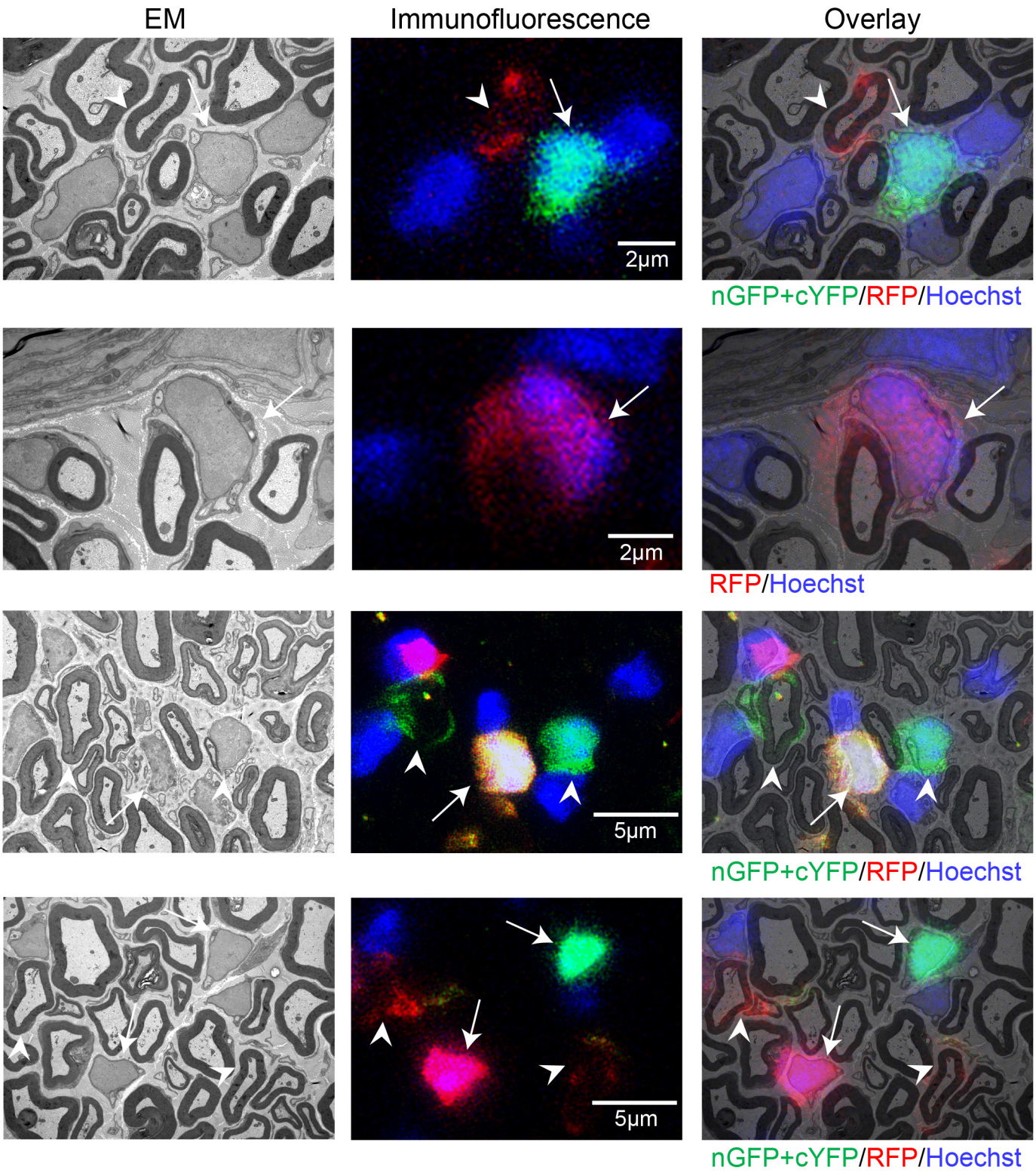

Figure S7, related to Figure 7. mSCs retain a SC fate following nerve injury but can switch to become a nmSC.

A series of Correlative Light and Electron Microscopy (CLEM) images of 200μm transverse sections of sciatic nerve isolated from P0-CreER^{T2}:Confetti mice, Day 90 after nerve transection, showing cytoplasmic RFP (red), nuclear GFP and cytoplasmic YFP (green) labelled mSCs that have redifferentiated to become nmSCs following injury. Panels show the EM image (left), the corresponding confocal image (middle) and the overlayed images (right). Arrowheads indicate labelled mSCs and arrows indicate mSC-derived cells that have differentiated into nmSCs.

Supplementary Information

Supplementary Materials and Methods

Immunostaining

After fixation in PFA, nerves were cryoprotected in 30% sucrose (w/v) in PBS overnight at 4ºC. The nerves were then transferred to a 1:1 mixture of 30% sucrose with O.C.T compound (TissueTek, Sakura) for 2 hours at RT and finally embedded in O.C.T before being snap-frozen in liquid nitrogen. 10-25µm longitudinal or transverse cryosections (Leica) were permeabilised in 0.3% Triton-X100 in PBS for 30 min, blocked in 10% goat serum/PBS for ≥1 hour and incubated in primary antibodies diluted in blocking buffer overnight (O/N) at 4°C. Sections were washed 3 times with PBS and the appropriate fluorescent secondary antibodies were used with Hoechst to counterstain the nuclei for 1h at RT. Samples were mounted in Fluoromount G (Southern Biotechnology) before imaging. Sciatic nerves from P0-CreER^{TR}:Confetti mice were fixed in Antigenfix (DiaPath) to preserve the endogenous fluorescence and RedDot (Biotium) or To-Pro-3 (Thermo Fisher Cat# T3605) was used as a nuclear counterstain. For better preservation of axonal proteins, PBS containing 1mM $CaCl_2$, 0.5mM $MgCl_2$ was used when needed. For P0 staining, harvested sciatic nerves were instead immediately snap frozen in liquid nitrogen. After cutting 10-25µm transverse cryosections, the sections were postfixed for 10min using 4% PFA at RT and washed thoroughly with PBS before blocking with 10% goat serum/PBS. The rest of the immunostaining protocol was as the staining protocol for the prefixed nerve.

Correlative light and electron microscopy (CLEM)

200µm vibrotome sections were screened using a widefield fluorescence microscope to identify sections containing a large number of fluorescently-labelled cells. These sections were imaged with a 40x lens using a SP8 confocal microscope (Leica). YFP, GFP and RFP was acquired (CFP excitation is not possible on this microscope. After image acquisition, samples were fixed in 2% (wt/vol) PFA, 1.5% (wt/vol) glutaraldehyde (both EM grade from TAAB) in 0.1M sodium cacodylate buffer for 30 mins at RT. Samples were then secondarily fixed in 1% (wt/vol) osmium tetroxide, 1.5% (wt/vol) potassium ferricyanide for 1h at 4 °C. After washes in 0.1M sodium cacodylate, samples were incubated in 1% (wt/vol) tannic acid in 0.5M sodium cacodylate at room temperature for 45 min. Further washes in 0.5M sodium cacodylate were followed by a final wash in distilled water, before the samples underwent dehydration by sequential short incubations in 70% (vol/vol) and 90% (vol/vol) ethanol and then two longer incubations in 100% ethanol. Samples were transferred to a 1:1 mix of propylene oxide and Epon resin (TAAB) for 90 min, then 100% Epon for two more incubations, one of several hours and one O/N. Finally samples were polymerised by baking at 60°C O/N. It is important that the side of the sample that was imaged by confocal microscopy faces the top of the

resulting resin block to ensure correlation between LM images and EM section images. Ultrathin sections were collected and imaged as above.

Image quantification analysis

Cell composition:

For the cell type quantifications, z-stack projections with an equal number of z-stacks were used. 4 or more non-overlapping fields of each section were imaged using a 63x objective on a SPE microscope. Three different sections were quantified per mouse (≥4 animals per group). The area of each quantified field was 0.0135mm^2. Confocal images were counted manually using Fiji software. Within TEM images, each cell type was identified and quantified based on their morphology and the presence of a nucleus. mSCs, nmSCs, pericytes and endothelial cells are morphologically very different, however, we were unable to differentiate between the pericyte-like cells and macrophages. Therefore these cell types were quantified as a single category.

Determination of proliferation rates

Turnover of each cell-type was determined by using measurements taken following 30 days of continuous EdU administration. The calculation used was: proportion of each cell-type/(proportion of each proliferating cell-type x the total proliferation rate at 30 days).

ECM analysis:

For area measurements, 4 or more different fields of each section were imaged, with three sections counted for each mouse (≥4 mice per group). Images were converted to 8-bit grey scale TIFF images using Fiji software. Each image was thresholded and made binary. The thresholded area was outlined using the "Create Selection" function and the immunostained area quantified using the measurement function. For intensity measurements, projections used an equal number of z-stacks. The intensity of 9 different fields per image was measured and averaged using Fiji software (3 images were acquired for each section, 3 sections per animal, 6 animals per group).

Axon quantification:

The diameter of individual axons measured from 6 images per mouse and 8 mice per group was binned to assess distribution. All measurements were done with Photoshop to draw the axons and Fiji software was used to measure their diameter. Total number of myelinated axons were counted from 3 imaged sections of the entire nerve per mouse (n= 5 mice per group).

Table S1: Antibodies

Antibodies	Source	Identifier
Chicken polyclonal anti myelin protein zero (P0)	Abcam	Cat# ab39375 RRID: AB_881430
Rabbit polyclonal anti-nerve growth factor (NGF-receptor) p75	Millipore	Cat# AB1554 RRID: AB_90760
Rabbit polyclonal S100	DAKO	Cat# Z0311 RRID: AB_10013383
Rabbit polyclonal anti-Iba1	WAKO	Cat# 019-19741 RRID: AB_839504
Rat anti-mouse CD31 platelet endothelial cell adhesion molecule (PECAM)	BD Biosciences	Cat# 553370 RRID: AB_394816
Chicken polyclonal anti-200kD neurofilament	Abcam	Cat# ab4680 RRID: AB_30456
Rabbit polyclonal anti-laminin	Abcam	Cat# ab11575 RRID: AB_298179
Rabbit polyclonal anti-collagen III	Abcam	Cat# ab7778 RRID: AB_306066
Mouse anti-human fibronectin	Sigma-Aldrich	Cat# FN-3E2 RRID: AB_476981
Rabbit polyclonal anti-NG2 chondroitin sulfate proteoglycan antibody	Abcam	Cat# ab5320 RRID: AB_11213678
Rabbit monoclonal anti-PDGF Receptor Beta (Y92)	Abcam	Cat# ab 32570 RRID: AB_777165
Mouse monoclonal anti-actin alpha-smooth muscle- Cy3 conjugated (Clone 1A4)	Sigma-Aldrich	Cat# C6198 RRID: AB_476856
Chicken polyclonal anti-GFP	Abcam	Cat# ab13970 RRID: AB_300798
Rabbit polyclonal anti-glucose transporter 1 (GLUT1)	Abcam	Cat# ab652 RRID: AB_305540
Rat anti-mouse F4/80	Bio-Rad / AbD Serotec	Cat# MCA497G RRID: AB_872005
Rat monoclonal anti-NG2 chondroitin sulfate proteoglycan antibody	Thermo Fisher	Cat# MA5-24247 RRID:AB_2606388

Table S2: Transgenic mice

Mice strains	Reference	Identifier
Mouse: P0A-Cre (P0-Cre)		RRID: IMSR_RBRC01459
Mouse: PLP-eGFP	(Mallon et al., 2002)	N/A
Mouse: NG2-dsRedBAC (NG2-dsRed)	(Zhu et al., 2008)	RRID: IMSR_JAX:008241
Mouse: B6.Cg-*Gt(ROSA)26Sor*$^{tm9(CAG-tdTomato)Hze}$ (R26R-tdTomato)		RRID: IMSR_JAX:007909
Mouse: Tg(Mpz-cre/ERT2)2Ueli (P0-CreER^{T2})	(Leone et al., 2003)	RRID: IMSR_ MGI: 2663097
Mouse: R26R-YFP	(Srinivas et al., 2001)	
Mouse: Gt(ROSA)26Sor$^{tm1(CAG-Brainbow2.1)Cle}$ (R26R-Confetti)	(Snippert et al., 2010)	RRID: IMSR_JAX:013731
Mouse: P0-CreER^{T2}:R26R-YFP:Nf1$^{fl/fl}$	(Ribeiro et al., 2013)	

Table S3: Genotyping primers

Genotyping primers		
Primer for genotyping: P0-Cre 1: CGGTCGATGCAACGAGTGATGAG	This paper	N/A
Primer for genotyping: P0-Cre 2: CCAGAGACGGAAATCCATCGCTC	This paper	N/A
Primer for genotyping: NF1 Common CTT CAG ACT GAT TGT TGT ACC TGA		RRID: IMSR_JAX:017639
Primer for genotyping: NF1 Wild Type Reverse ACC TCT CTA GCC TCA GGA ATG A		RRID: IMSR_JAX:017639
Primer for genotyping: NF1 Mutant Reverse TGA TTC CCA CTT TCT GGT TCT AAG		RRID: IMSR_JAX:017639
Primer for genotyping: Confetti Mutant Forward GAA TTA ATT CCG GTA TAA CTT CG		RRID: IMSR_JAX:013731
Primer for genotyping: Confetti Wild Type Forward AAA GTC GCT CTG AGT TGT TA		RRID: IMSR_JAX:013731
Primer for genotyping: Confetti common CCA GAT GAC TAC CTA TCC TC		RRID: IMSR_JAX:013731
Primer for genotyping: R26R Mutant Reverse GCG AAG AGT TTG TCC TCA ACC-3	(Srinivas et al., 2001)	
Primer for genotyping: R26R Reverse GGA GCG GGA GAA ATG GAT ATG	(Srinivas et al., 2001)	
Primer for genotyping: R26R Common AAA GTC GCT CTG AGT TGT TAT	(Srinivas et al., 2001)	
Primer for genotyping: Tomato Wild Type Forward AAG GGA GCT GCA GTG GAG TA		RRID: IMSR_JAX:007909
Primer for genotyping: Tomato Wild Type Reverse CCG AAA ATC TGT GGG AAG TC		RRID: IMSR_JAX:007909
Primer for genotyping: Tomato Mutant Reverse GGC ATT AAA GCA GCG TAT CC		RRID: IMSR_JAX:007909
Primer for genotyping: Tomato Mutant Forward CTG TTC CTG TAC GGC ATG G		RRID: IMSR_JAX:007909
Primer for genotyping: Forward TTC CTT CGC CTT ACA AGT CC		RRID: IMSR_JAX:008241
Primer for genotyping: Reverse GAG CCG TAC TGG AAC TGG		RRID: IMSR_JAX:008241

Supplementary References

Leone, D. P., Genoud, S., Atanasoski, S., Grausenburger, R., Berger, P., Metzger, D., Macklin, W. B., Chambon, P. and Suter, U. (2003). Tamoxifen-inducible glia-specific Cre mice for somatic mutagenesis in oligodendrocytes and Schwann cells. *Molecular and cellular neurosciences* **22**, 430-440.

Mallon, B. S., Shick, H. E., Kidd, G. J. and Macklin, W. B. (2002). Proteolipid promoter activity distinguishes two populations of NG2-positive cells throughout neonatal cortical development. *The Journal of neuroscience : the official journal of the Society for Neuroscience* **22**, 876-885.

Ribeiro, S., Napoli, I., White, I. J., Parrinello, S., Flanagan, A. M., Suter, U., Parada, L. F. and Lloyd, A. C. (2013). Injury signals cooperate with Nf1 loss to relieve the tumor-suppressive environment of adult peripheral nerve. *Cell reports* **5**, 126-136.

Snippert, H. J., van der Flier, L. G., Sato, T., van Es, J. H., van den Born, M., Kroon-Veenboer, C., Barker, N., Klein, A. M., van Rheenen, J., Simons, B. D., et al. (2010). Intestinal crypt homeostasis results from neutral competition between symmetrically dividing Lgr5 stem cells. *Cell* **143**, 134-144.

Srinivas, S., Watanabe, T., Lin, C. S., William, C. M., Tanabe, Y., Jessell, T. M. and Costantini, F. (2001). Cre reporter strains produced by targeted insertion of EYFP and ECFP into the ROSA26 locus. *BMC developmental biology* **1**, 4.

Zhu, X., Bergles, D. E. and Nishiyama, A. (2008). NG2 cells generate both oligodendrocytes and gray matter astrocytes. *Development* **135**, 145-157.

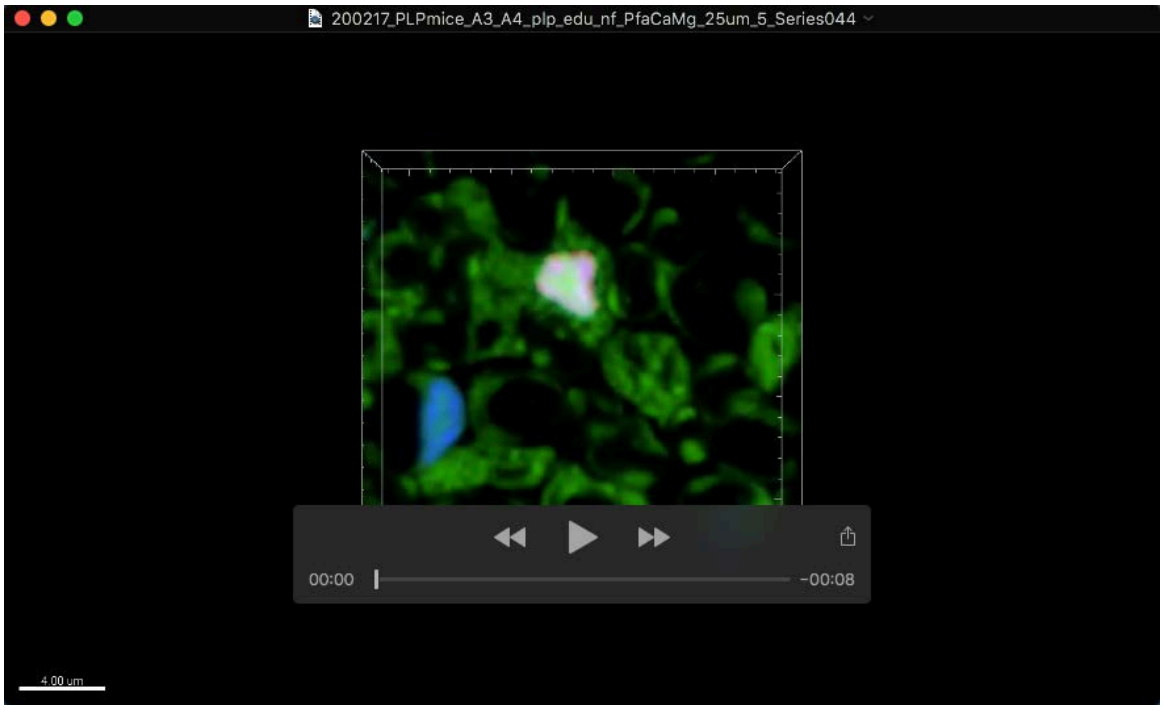

Movie 1: Non myelinating Schwann cells proliferate slowly in adult peripheral nerve.

Movie shows a rotating 3D projection of Z-stacks of confocal images of a transverse section ((20µm) of a sciatic nerve isolated from a PLP-eGFP mouse that had been treated with EdU continuously for 30 days prior to culling. The images were processed using Imaris software. The movie highlights a EdU+ (red), non-myelinating Schwann cell (eGFP+) associated with small calibre axons (neurofilament, white).

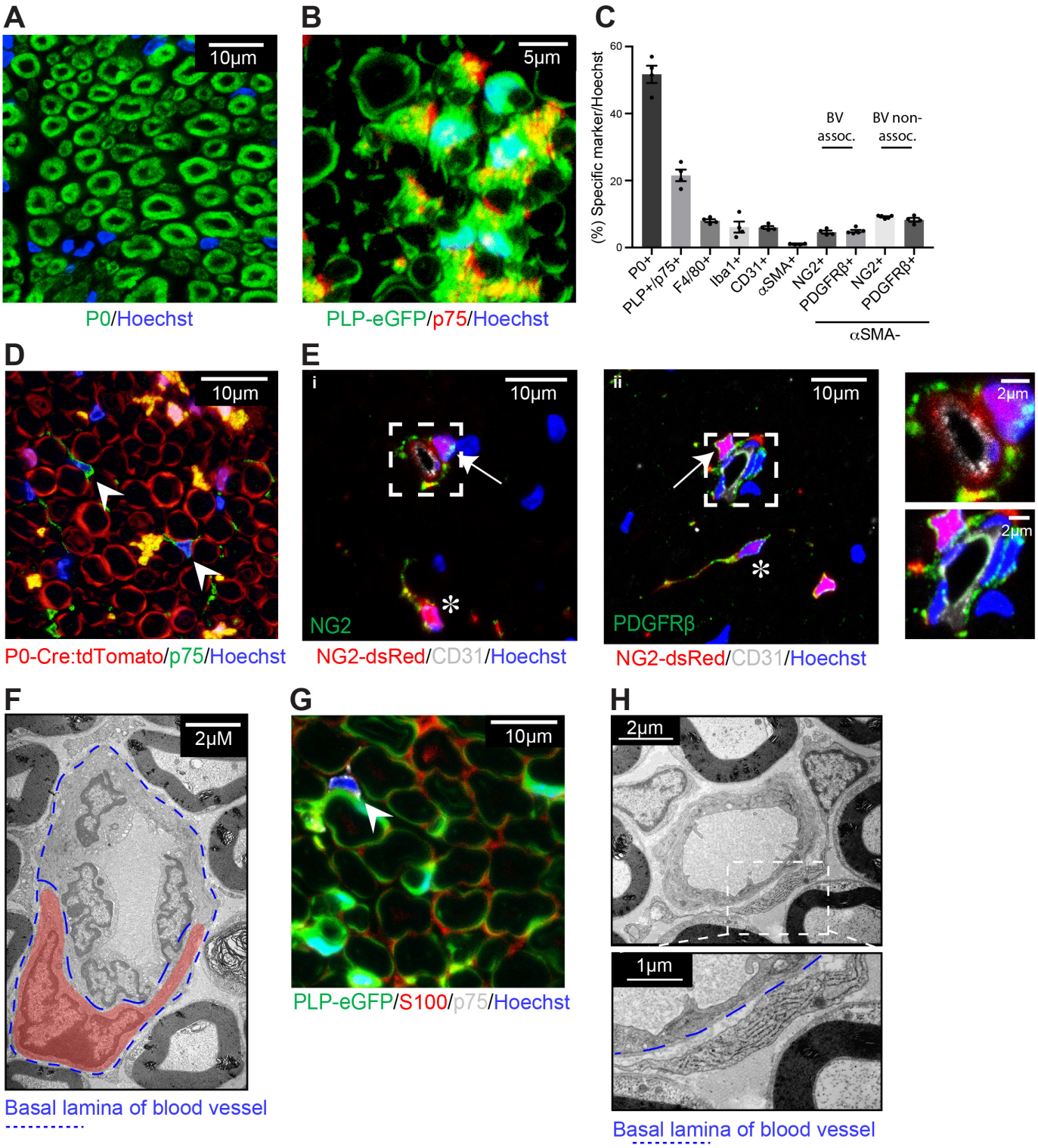

Figure S1, related to Figure 1. Identification of the cell composition of peripheral nerve.
Representative confocal images of **A)** mSCs (P0+) and **B)** nmSCs (PLP+/ p75+). **C)** Graph shows the quantification of specific markers expressed by cells in sciatic nerve (n=4-5 mice, mean±SEM). Pericytes are defined by the co-expression of NG2, PDGFRß and αSMA. A separate population is NG2/ PDGFRß+ but αSMA-. These cells were further characterised as associated or non-associated with CD31+ blood vessels (BV). **D)** Representative confocal image shows a transverse section of a sciatic nerve isolated from a P0-Cre:tdTomato mouse immunostained for p75 (green). Arrowheads indicate tdTomato-/ p75+ cells. **E)** Sections from NG2-dsRed mice were co-stained for (i) NG2 (green) and (ii) PDGFRß (green). Arrows indicate CD31+ - associated cells, asterisks indicate a CD31+ non-associated population. White rectangles indicate the regions that are shown at higher magnifiation on the right. **F)** Representative EM image showing a classical pericyte (red), which is in tight contact with a blood vessel and is within the basal lamina. **G)** Transverse section of a sciatic nerve isolated from a PLP-eGFP mouse immunostained for p75 (grey) and S100 (red). Arrowhead indicates an eGFP-/S100-/p75+ cell. **H)** Representative EM images show an elongated cell, rich in endoplasmic reticulum, closely associated with a blood vessel. The higher magnification image shows that it is not surrounded by the basal lamina.

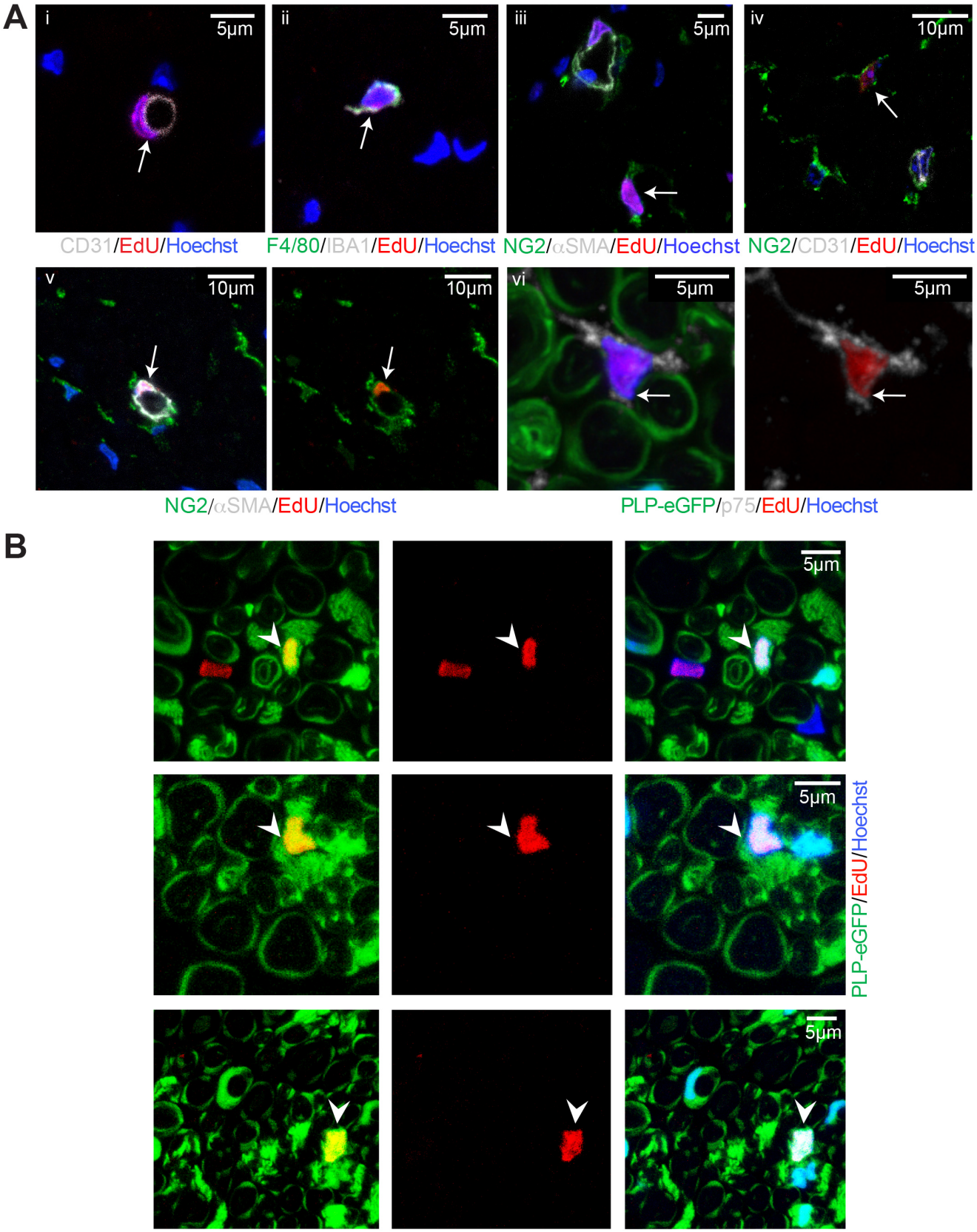

Figure S2, related to Figure 2. Peripheral nerve is a highly quiescent tissue.
A) Representative confocal images of (i-v) transverse sections of sciatic nerve from WT mice and (vi) PLP-eGFP mice treated continuously with EdU for 30 days, processed to detect EdU (red) and immunolabelled for (i) CD31, to detect endothelial cells (white). (ii) F4/80 (green)/ Iba1 (white), to detect macrophages. (iii) NG2 (green) and αSMA (white) to detect pericytes. (iv) NG2 (green), and CD31 (white) to detect NG2+ cells non-associated with CD31+ blood vessels. (v) NG2 (green) and αSMA (white). (vi) p75 (white) to detect PLP-/ p75+/ EdU+ cells. Nuclei are stained with Hoechst (blue). Arrows indicate proliferating cells. **B)** Confocal images of 20μm cryosections of sciatic nerve isolated from PLP-eGFP mice treated continuously with EdU (red) for 30 days. Nuclei are stained with Hoechst (blue). Arrowheads indicate three separate examples of proliferating nmSCs (PLP+/ EdU+).

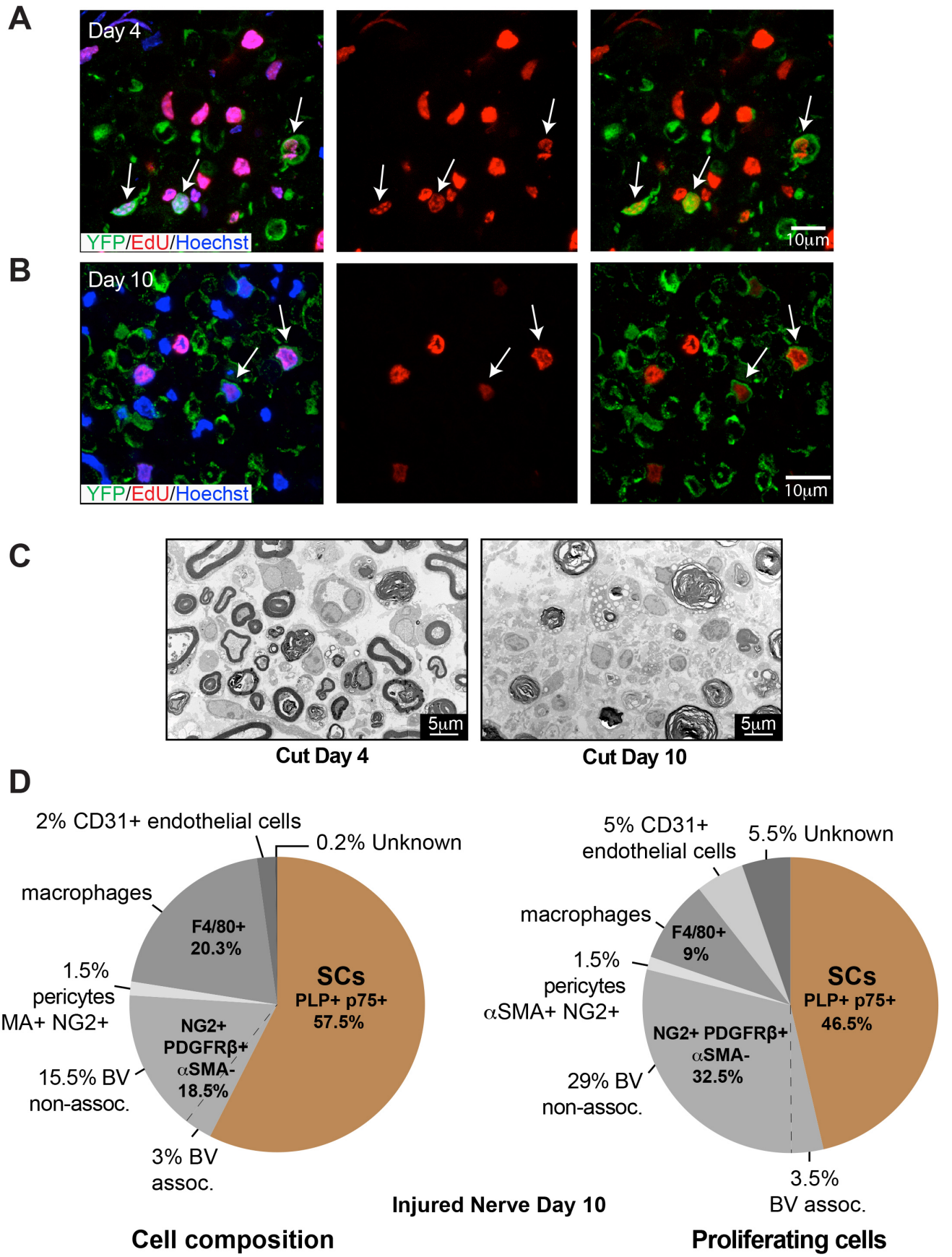

Figure S3, related to Figure 3. All mSCs proliferate following injury.
A-B) Representative confocal images of transverse sections of transected sciatic nerve of P0-CreER^{T2}:YFP mice in which mSCs were labelled with YFP following Tmx administration. Arrows indicate Edu+/ YFP+ cells **A)** Day 10 following injury, EdU was administered continuously in the drinking water. **B)** Day 4 following injury, EdU was injected 3 hours prior to harvesting. **C)** Representative EM images of the distal stump of injured sciatic nerves at Day 4 and Day 10 following transection. **D)** Pie charts show the cell composition and the relative proportions of the cell types proliferating in the distal stump of an injured sciatic nerve at Day 10 following injury (n=8 mice).

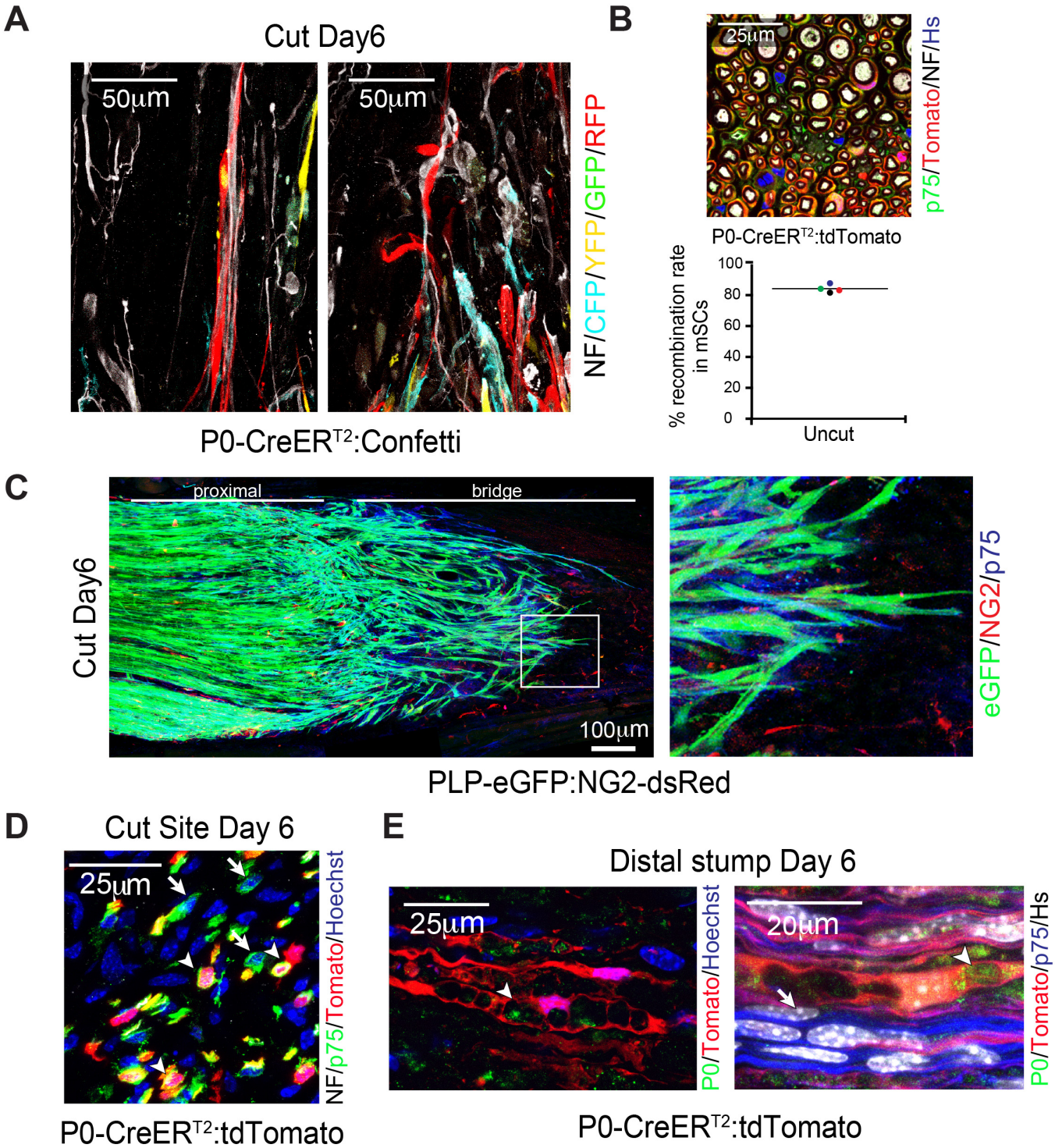

Figure S4, related to Figure 4 : mSCs become migratory following injury to guide regrowing axons.
A) Representative images of a longitudinal cryosection of an injured sciatic nerve of P0-CreER^{T2}:Confetti mice, Day 6 following injury, shows migrating SCs derived from mSCs associated with regrowing axons in the nerve bridge. An antibody to neurofilament (NF) was used to label the axons. **B)** Representative image of a transverse cryosection of uninjured sciatic nerves of P0-CreER^{T2}:tdTomato mice following tamoxifen administration. Antibodies to S100 and neurofilament (NF) were used to label SCs and axons, respectively. Graph shows the percentage of recombined mSCs and shows that more than 80% of mSCs express Tomato following tamoxifen administration. Each coloured dot represents an individual animal. Line shows mean±SEM. **C)** Representative image of a longitudinal cryosection of the bridge region (Cut site) of an injured sciatic nerve from PLP-eGFP:NG2-dsRed mice, Day 6 following injury. An Antibody to p75 was used to label dedifferentiated SCs. **D)** Representative image of a transverse cryosection of the bridge region (Cut site) of an injured sciatic nerve from P0-CreER^{T2}:tdTomato mice, Day 6 following injury. Antibodies to p75 and neurofilament (NF) were used to label dedifferentiated SCs and axons, respectively. Arrowheads indicate Tomato+/p75+ cells and arrows Tomato-/p75+ cells and show that SCs derived from mSCs are associated with axons in the bridge region. **E)** Representative images of a longitudinal section of the distal stump of P0-CreER^{T2}:tdTomato mice, showing that SCs derived from mSCs engulf and degrade myelin debris. Antibodies to P0 and p75 weres used to label dedifferentiated SCs and the degraded myelin, respectively. Arrowheads indicate myelin debris that has been engulfed by myelinating Schwann cell derived cells and the arrow indicates a Tomato-/P75+ cell devoid of myelin debris.

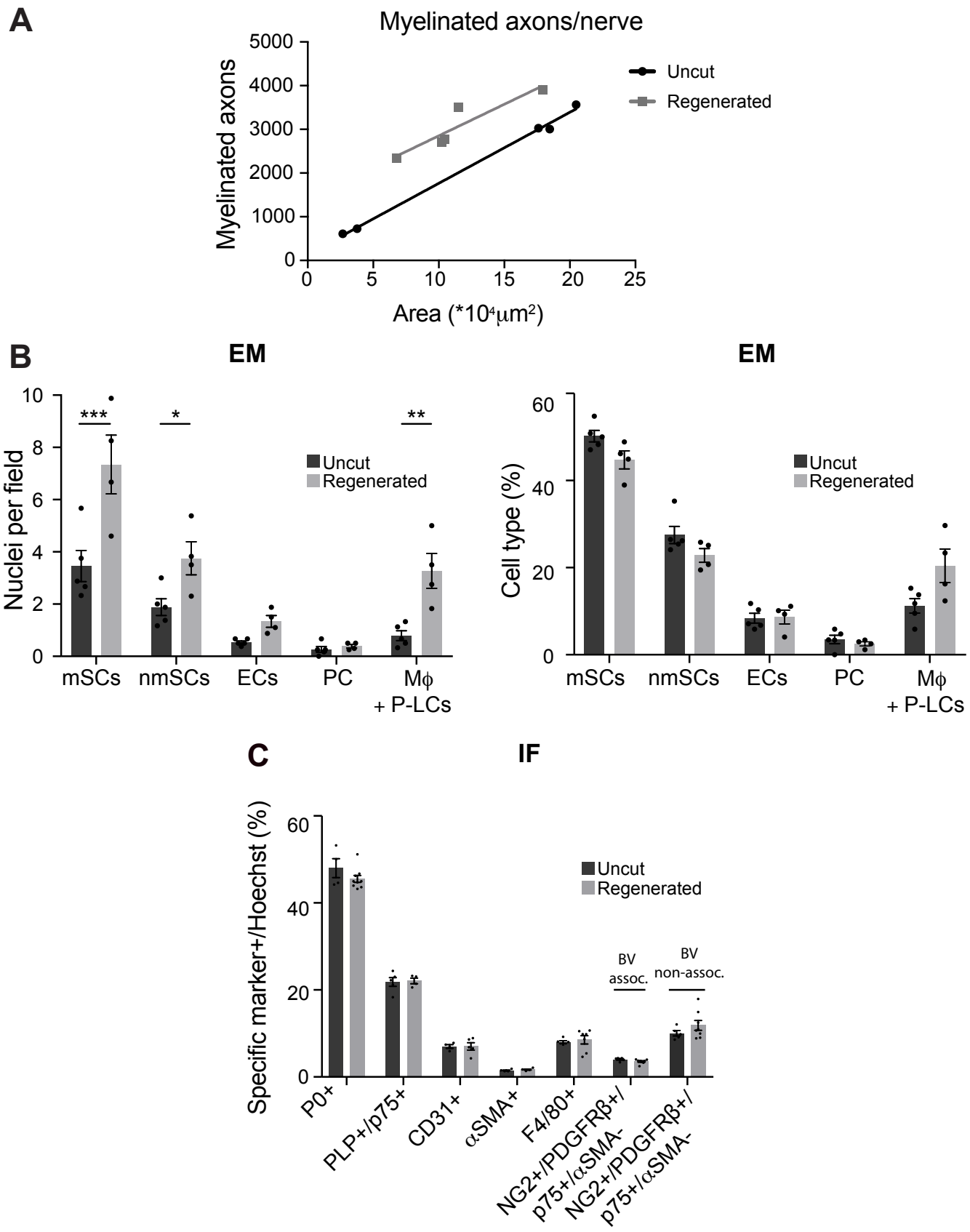

Figure S5, related to Figure 5. Regenerated nerve is distinct from uninjured nerve.
A) Graph shows the quantification of the total number of axons in uncut and regenerated nerve. Each point represents an individual nerve. **B)** Quantification of EM images showing the number of specific cell types per field (LHS) and the proportion of each cell type (RHS) in uncut and regenerated nerves, 6 months following injury. Cells were identified by morphology. EC (endothelial cells), PC (pericytes). We were not confident distinguishing macrophages (Mϕ) from NG2+/ PDGFRβ/ P75+ cells, labelled as P-LCs (pericyte-like cells) in the EM quantifications, and so these cells were grouped together (n=4-5 mice, mean±SEM, two-way ANNOVA was used). **C)** Quantification of immunofluorescent images showing the proportion of each cell type, identified by the indicated markers, in the uncut and regenerated nerves, 6 months following injury (n=4-9 mice, mean±SEM).

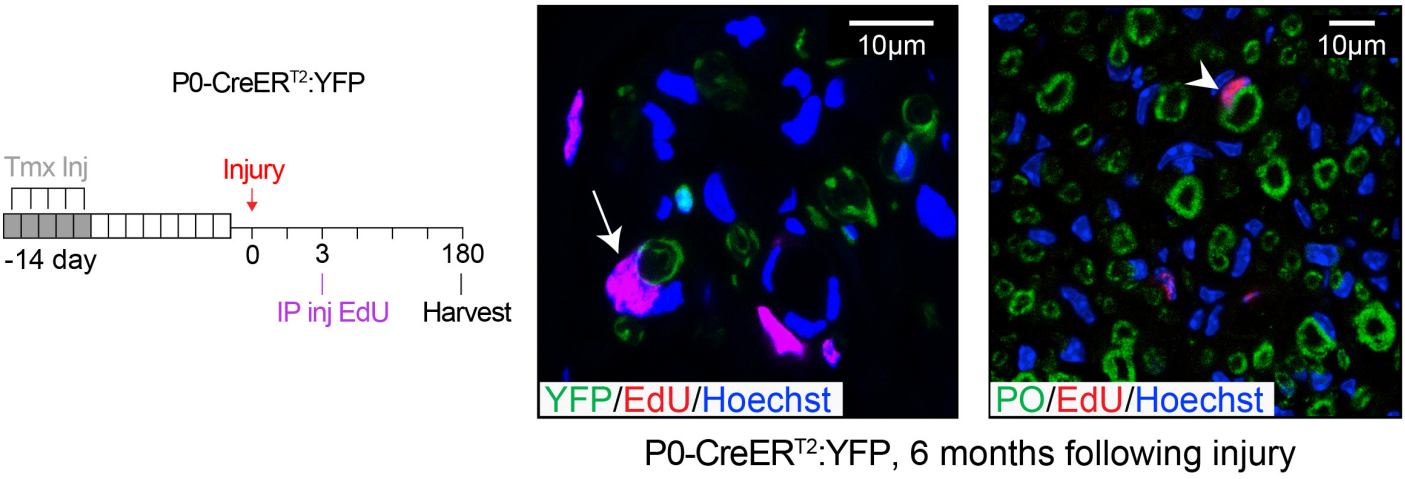

Figure S6, related to Figure 7. mSCs retain a SC fate following nerve injury but can switch to become a nmSC.
Schematic representation of the protocol used to determine whether proliferating cells derived from mSCs remyelinate axons. P0-CreER^{T2}:YFP mice were injected intraperitoneally with Tmx for 5 consecutive days. 14 days following the first injection, the right sciatic nerve was cut and EdU was injected at Day 3 following injury. Mice were harvested 6 months later. Representative confocal images show transverse sections from the regenerated nerve of EdU injected P0-CreER^{T2}:YFP mice, 6 months following injury. The arrow indicates a YFP+ mSC that proliferated at Day 3 following injury and redifferentiated into a mSC. The arrowhead indicates a cell that proliferated at Day 3 following injury and became a mSC, as indicated by P0 staining.

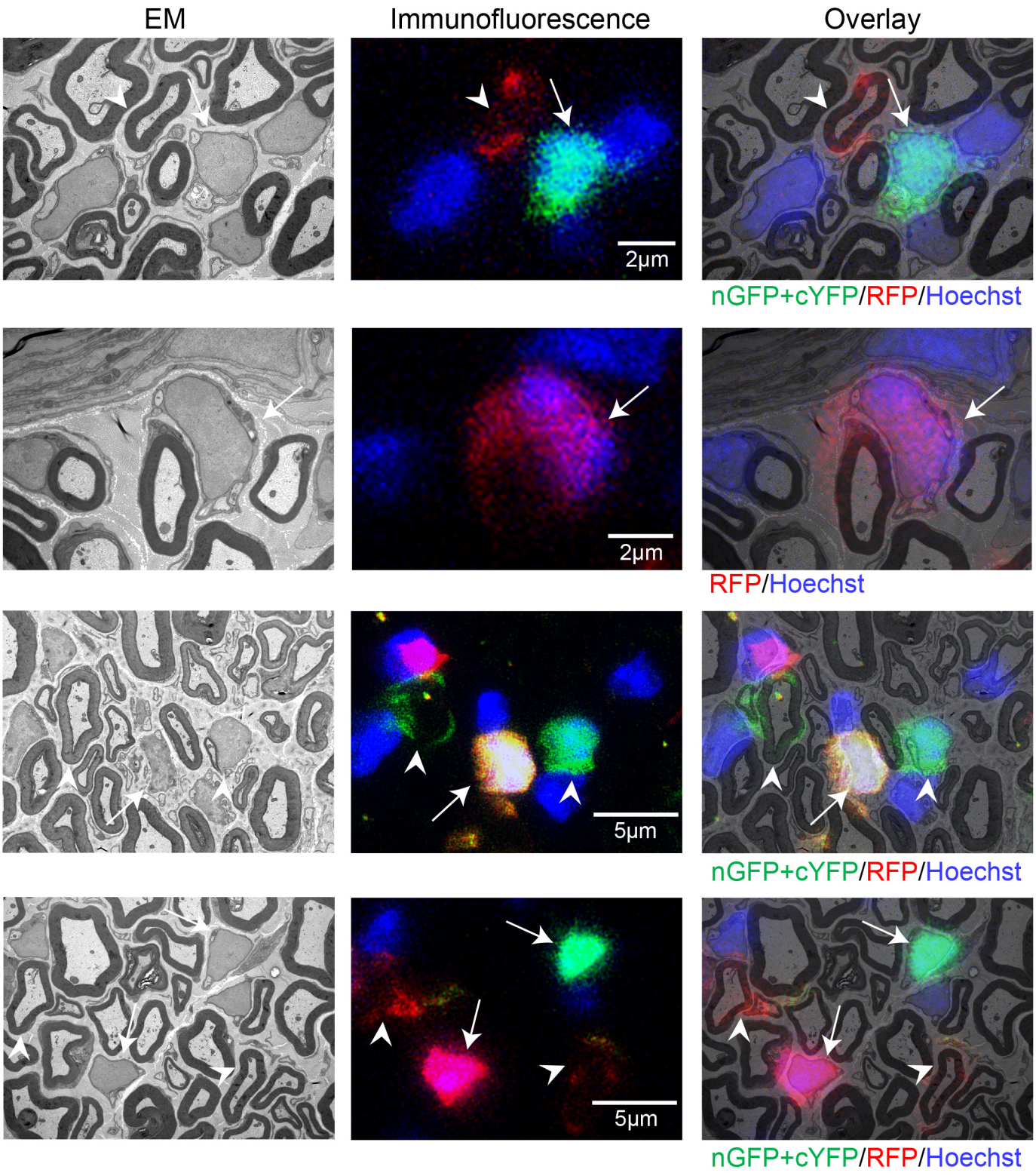

Figure S7, related to Figure 7. mSCs retain a SC fate following nerve injury but can switch to become a nmSC.

A series of Correlative Light and Electron Microscopy (CLEM) images of 200μm transverse sections of sciatic nerve isolated from P0-CreER^{T2}:Confetti mice, Day 90 after nerve transection, showing cytoplasmic RFP (red), nuclear GFP and cytoplasmic YFP (green) labelled mSCs that have redifferentiated to become nmSCs following injury. Panels show the EM image (left), the corresponding confocal image (middle) and the overlayed images (right). Arrowheads indicate labelled mSCs and arrows indicate mSC-derived cells that have differentiated into nmSCs.

Supplementary Information

Supplementary Materials and Methods

Immunostaining

After fixation in PFA, nerves were cryoprotected in 30% sucrose (w/v) in PBS overnight at 4ºC. The nerves were then transferred to a 1:1 mixture of 30% sucrose with O.C.T compound (TissueTek, Sakura) for 2 hours at RT and finally embedded in O.C.T before being snap-frozen in liquid nitrogen. 10-25µm longitudinal or transverse cryosections (Leica) were permeabilised in 0.3% Triton-X100 in PBS for 30 min, blocked in 10% goat serum/PBS for ≥1 hour and incubated in primary antibodies diluted in blocking buffer overnight (O/N) at 4°C. Sections were washed 3 times with PBS and the appropriate fluorescent secondary antibodies were used with Hoechst to counterstain the nuclei for 1h at RT. Samples were mounted in Fluoromount G (Southern Biotechnology) before imaging. Sciatic nerves from P0-CreER^{TR}:Confetti mice were fixed in Antigenfix (DiaPath) to preserve the endogenous fluorescence and RedDot (Biotium) or To-Pro-3 (Thermo Fisher Cat# T3605) was used as a nuclear counterstain. For better preservation of axonal proteins, PBS containing 1mM $CaCl_2$, 0.5mM $MgCl_2$ was used when needed. For P0 staining, harvested sciatic nerves were instead immediately snap frozen in liquid nitrogen. After cutting 10-25µm transverse cryosections, the sections were postfixed for 10min using 4% PFA at RT and washed thoroughly with PBS before blocking with 10% goat serum/PBS. The rest of the immunostaining protocol was as the staining protocol for the prefixed nerve.

Correlative light and electron microscopy (CLEM)

200µm vibrotome sections were screened using a widefield fluorescence microscope to identify sections containing a large number of fluorescently-labelled cells. These sections were imaged with a 40x lens using a SP8 confocal microscope (Leica). YFP, GFP and RFP was acquired (CFP excitation is not possible on this microscope. After image acquisition, samples were fixed in 2% (wt/vol) PFA, 1.5% (wt/vol) glutaraldehyde (both EM grade from TAAB) in 0.1M sodium cacodylate buffer for 30 mins at RT. Samples were then secondarily fixed in 1% (wt/vol) osmium tetroxide, 1.5% (wt/vol) potassium ferricyanide for 1h at 4 °C. After washes in 0.1M sodium cacodylate, samples were incubated in 1% (wt/vol) tannic acid in 0.5M sodium cacodylate at room temperature for 45 min. Further washes in 0.5M sodium cacodylate were followed by a final wash in distilled water, before the samples underwent dehydration by sequential short incubations in 70% (vol/vol) and 90% (vol/vol) ethanol and then two longer incubations in 100% ethanol. Samples were transferred to a 1:1 mix of propylene oxide and Epon resin (TAAB) for 90 min, then 100% Epon for two more incubations, one of several hours and one O/N. Finally samples were polymerised by baking at 60°C O/N. It is important that the side of the sample that was imaged by confocal microscopy faces the top of the

resulting resin block to ensure correlation between LM images and EM section images. Ultrathin sections were collected and imaged as above.

Image quantification analysis

Cell composition:

For the cell type quantifications, z-stack projections with an equal number of z-stacks were used. 4 or more non-overlapping fields of each section were imaged using a 63x objective on a SPE microscope. Three different sections were quantified per mouse (≥4 animals per group). The area of each quantified field was 0.0135mm^2. Confocal images were counted manually using Fiji software. Within TEM images, each cell type was identified and quantified based on their morphology and the presence of a nucleus. mSCs, nmSCs, pericytes and endothelial cells are morphologically very different, however, we were unable to differentiate between the pericyte-like cells and macrophages. Therefore these cell types were quantified as a single category.

Determination of proliferation rates

Turnover of each cell-type was determined by using measurements taken following 30 days of continuous EdU administration. The calculation used was: proportion of each cell-type/(proportion of each proliferating cell-type x the total proliferation rate at 30 days).

ECM analysis:

For area measurements, 4 or more different fields of each section were imaged, with three sections counted for each mouse (≥4 mice per group). Images were converted to 8-bit grey scale TIFF images using Fiji software. Each image was thresholded and made binary. The thresholded area was outlined using the "Create Selection" function and the immunostained area quantified using the measurement function. For intensity measurements, projections used an equal number of z-stacks. The intensity of 9 different fields per image was measured and averaged using Fiji software (3 images were acquired for each section, 3 sections per animal, 6 animals per group).

Axon quantification:

The diameter of individual axons measured from 6 images per mouse and 8 mice per group was binned to assess distribution. All measurements were done with Photoshop to draw the axons and Fiji software was used to measure their diameter. Total number of myelinated axons were counted from 3 imaged sections of the entire nerve per mouse (n= 5 mice per group).

Table S1: Antibodies

Antibodies	Source	Identifier
Chicken polyclonal anti myelin protein zero (P0)	Abcam	Cat# ab39375 RRID: AB_881430
Rabbit polyclonal anti-nerve growth factor (NGF-receptor) p75	Millipore	Cat# AB1554 RRID: AB_90760
Rabbit polyclonal S100	DAKO	Cat# Z0311 RRID: AB_10013383
Rabbit polyclonal anti-Iba1	WAKO	Cat# 019-19741 RRID: AB_839504
Rat anti-mouse CD31 platelet endothelial cell adhesion molecule (PECAM)	BD Biosciences	Cat# 553370 RRID: AB_394816
Chicken polyclonal anti-200kD neurofilament	Abcam	Cat# ab4680 RRID: AB_30456
Rabbit polyclonal anti-laminin	Abcam	Cat# ab11575 RRID: AB_298179
Rabbit polyclonal anti-collagen III	Abcam	Cat# ab7778 RRID: AB_306066
Mouse anti-human fibronectin	Sigma-Aldrich	Cat# FN-3E2 RRID: AB_476981
Rabbit polyclonal anti-NG2 chondroitin sulfate proteoglycan antibody	Abcam	Cat# ab5320 RRID: AB_11213678
Rabbit monoclonal anti-PDGF Receptor Beta (Y92)	Abcam	Cat# ab 32570 RRID: AB_777165
Mouse monoclonal anti-actin alpha-smooth muscle- Cy3 conjugated (Clone 1A4)	Sigma-Aldrich	Cat# C6198 RRID: AB_476856
Chicken polyclonal anti-GFP	Abcam	Cat# ab13970 RRID: AB_300798
Rabbit polyclonal anti-glucose transporter 1 (GLUT1)	Abcam	Cat# ab652 RRID: AB_305540
Rat anti-mouse F4/80	Bio-Rad / AbD Serotec	Cat# MCA497G RRID: AB_872005
Rat monoclonal anti-NG2 chondroitin sulfate proteoglycan antibody	Thermo Fisher	Cat# MA5-24247 RRID:AB_2606388

Table S2: Transgenic mice

Mice strains	Reference	Identifier
Mouse: P0A-Cre (P0-Cre)		RRID: IMSR_RBRC01459
Mouse: PLP-eGFP	(Mallon et al., 2002)	N/A
Mouse: NG2-dsRedBAC (NG2-dsRed)	(Zhu et al., 2008)	RRID: IMSR_JAX:008241
Mouse: B6.Cg-*Gt(ROSA)26Sor*$^{tm9(CAG-tdTomato)Hze}$ (R26R-tdTomato)		RRID: IMSR_JAX:007909
Mouse: Tg(Mpz-cre/ERT2)2Ueli (P0-CreER^{T2})	(Leone et al., 2003)	RRID: IMSR_ MGI: 2663097
Mouse: R26R-YFP	(Srinivas et al., 2001)	
Mouse: Gt(ROSA)26Sor$^{tm1(CAG-Brainbow2.1)Cle}$ (R26R-Confetti)	(Snippert et al., 2010)	RRID: IMSR_JAX:013731
Mouse: P0-CreER^{T2}:R26R-YFP:Nf1$^{fl/fl}$	(Ribeiro et al., 2013)	

Table S3: Genotyping primers

Genotyping primers		
Primer for genotyping: P0-Cre 1: CGGTCGATGCAACGAGTGATGAG	This paper	N/A
Primer for genotyping: P0-Cre 2: CCAGAGACGGAAATCCATCGCTC	This paper	N/A
Primer for genotyping: NF1 Common CTT CAG ACT GAT TGT TGT ACC TGA		RRID: IMSR_JAX:017639
Primer for genotyping: NF1 Wild Type Reverse ACC TCT CTA GCC TCA GGA ATG A		RRID: IMSR_JAX:017639
Primer for genotyping: NF1 Mutant Reverse TGA TTC CCA CTT TCT GGT TCT AAG		RRID: IMSR_JAX:017639
Primer for genotyping: Confetti Mutant Forward GAA TTA ATT CCG GTA TAA CTT CG		RRID: IMSR_JAX:013731
Primer for genotyping: Confetti Wild Type Forward AAA GTC GCT CTG AGT TGT TA		RRID: IMSR_JAX:013731
Primer for genotyping: Confetti common CCA GAT GAC TAC CTA TCC TC		RRID: IMSR_JAX:013731
Primer for genotyping: R26R Mutant Reverse GCG AAG AGT TTG TCC TCA ACC-3	(Srinivas et al., 2001)	
Primer for genotyping: R26R Reverse GGA GCG GGA GAA ATG GAT ATG	(Srinivas et al., 2001)	
Primer for genotyping: R26R Common AAA GTC GCT CTG AGT TGT TAT	(Srinivas et al., 2001)	
Primer for genotyping: Tomato Wild Type Forward AAG GGA GCT GCA GTG GAG TA		RRID: IMSR_JAX:007909
Primer for genotyping: Tomato Wild Type Reverse CCG AAA ATC TGT GGG AAG TC		RRID: IMSR_JAX:007909
Primer for genotyping: Tomato Mutant Reverse GGC ATT AAA GCA GCG TAT CC		RRID: IMSR_JAX:007909
Primer for genotyping: Tomato Mutant Forward CTG TTC CTG TAC GGC ATG G		RRID: IMSR_JAX:007909
Primer for genotyping: Forward TTC CTT CGC CTT ACA AGT CC		RRID: IMSR_JAX:008241
Primer for genotyping: Reverse GAG CCG TAC TGG AAC TGG		RRID: IMSR_JAX:008241

Supplementary References

Leone, D. P., Genoud, S., Atanasoski, S., Grausenburger, R., Berger, P., Metzger, D., Macklin, W. B., Chambon, P. and Suter, U. (2003). Tamoxifen-inducible glia-specific Cre mice for somatic mutagenesis in oligodendrocytes and Schwann cells. *Molecular and cellular neurosciences* **22**, 430-440.

Mallon, B. S., Shick, H. E., Kidd, G. J. and Macklin, W. B. (2002). Proteolipid promoter activity distinguishes two populations of NG2-positive cells throughout neonatal cortical development. *The Journal of neuroscience : the official journal of the Society for Neuroscience* **22**, 876-885.

Ribeiro, S., Napoli, I., White, I. J., Parrinello, S., Flanagan, A. M., Suter, U., Parada, L. F. and Lloyd, A. C. (2013). Injury signals cooperate with Nf1 loss to relieve the tumor-suppressive environment of adult peripheral nerve. *Cell reports* **5**, 126-136.

Snippert, H. J., van der Flier, L. G., Sato, T., van Es, J. H., van den Born, M., Kroon-Veenboer, C., Barker, N., Klein, A. M., van Rheenen, J., Simons, B. D., et al. (2010). Intestinal crypt homeostasis results from neutral competition between symmetrically dividing Lgr5 stem cells. *Cell* **143**, 134-144.

Srinivas, S., Watanabe, T., Lin, C. S., William, C. M., Tanabe, Y., Jessell, T. M. and Costantini, F. (2001). Cre reporter strains produced by targeted insertion of EYFP and ECFP into the ROSA26 locus. *BMC developmental biology* **1**, 4.

Zhu, X., Bergles, D. E. and Nishiyama, A. (2008). NG2 cells generate both oligodendrocytes and gray matter astrocytes. *Development* **135**, 145-157.

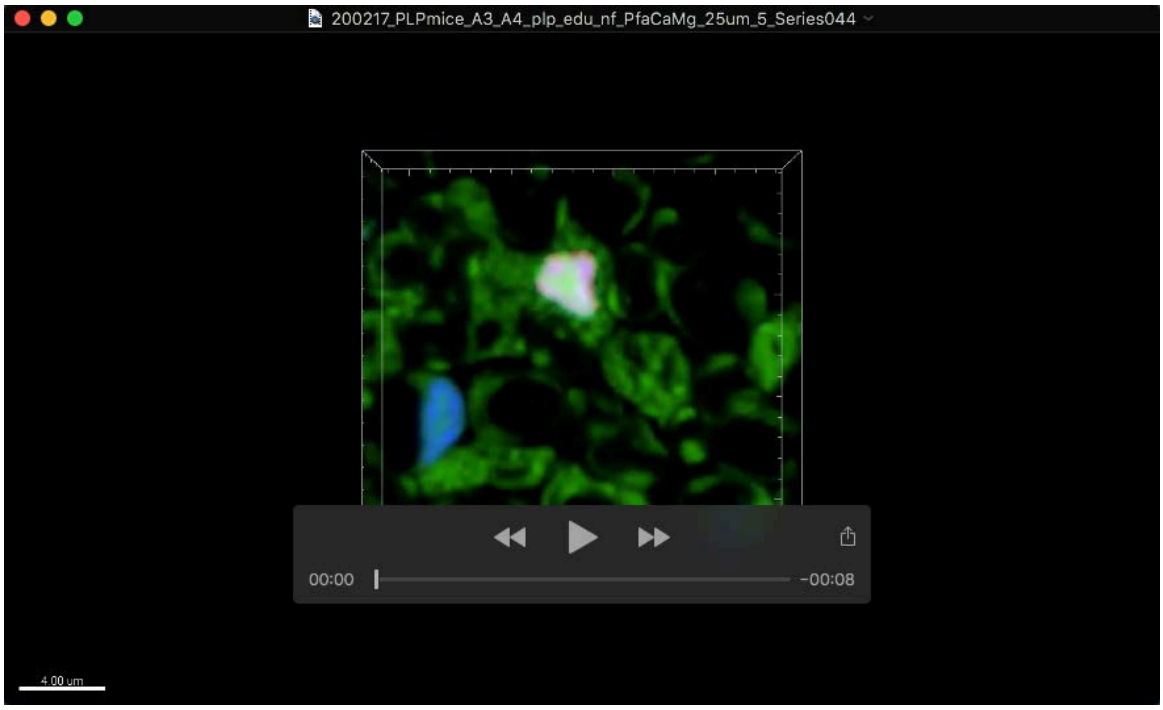

Movie 1: Non myelinating Schwann cells proliferate slowly in adult peripheral nerve.

Movie shows a rotating 3D projection of Z-stacks of confocal images of a transverse section ((20µm) of a sciatic nerve isolated from a PLP-eGFP mouse that had been treated with EdU continuously for 30 days prior to culling. The images were processed using Imaris software. The movie highlights a EdU+ (red), non-myelinating Schwann cell (eGFP+) associated with small calibre axons (neurofilament, white).